ORIGINAL ARTICLE

Evolving temperature field in a fossil subduction channel during the transition from subduction to collision (Tauern Window, Eastern Alps)

Philip Groß [ID] | **Jan Pleuger** | **Mark R. Handy** [ID] | **Marisa Germer** | **Timm John** [ID]

Institut für Geologische Wissenschaften, Freie Universität Berlin, Berlin, Germany

Correspondence
Freie Universität Berlin, Institut für Geologische Wissenschaften, Malteserstraße 74-100, 12249 Berlin, Germany.
Email: philip.gross@fu-berlin.de

Funding information
Deutsche Forschungsgemeinschaft, Grant/Award Number: HA 2403/24- 1, JO 349/11-1 and PL 534/4-1

Handling Editor: Katy Evans

Abstract

We investigate the evolution of the three-dimensional thermal structure of a palaeo-subduction channel exposed in the Penninic units of the central Tauern Window (Eastern Alps). Structural and petrological observations reveal a sheath fold with an amplitude of some 20 km that formed under high-P conditions (~2 GPa). The fold is a composite structure that isoclinally folded the thrust of an ophiolitic nappe derived from Alpine Tethys Ocean onto a unit of the distal European continental margin, also affected by the high-P conditions. This structural assemblage is preserved between two younger domes at either end of the Tauern Window. The domes deform isograds of the T-dominated Barrovian metamorphism that itself overprints the high-P metamorphism partly preserved in the sheath fold. Using Raman spectroscopy on carbonaceous material (RSCM), we are able to distinguish peak-temperature domains related to the original subduction metamorphism from domains associated with the later temperature-dominated (Barrovian) metamorphism. The distribution of RSCM temperatures in the Barrovian domain indicates a lateral and vertical decrease of peak temperature with increasing distance from the centres of the thermal domes. This represents a downward increase of palaeo-temperature, in line with previous studies. However, we observe the opposite palaeo-temperature trend in the lower limb of the sheath fold, namely an upward increase. We interpret this inverted palaeo-temperature domain as the relic of a subduction-related temperature field. Towards the central part of the sheath fold's upper limb, RSCM temperatures increase to a maximum of ~520°C. Further upsection in the hangingwall of the sheath fold, palaeo-peak temperatures decrease to where they are indistinguishable from the peak temperatures of the overprinting Barrovian metamorphism. Peak-temperature contours of the subduction-related metamorphism are oriented roughly parallel to the folded nappe contacts and lithological layering. The contours close towards the northern, western and eastern parts of the fold, resulting in an eye-shaped, concentric pattern in cross-section. The temperature contour geometry therefore mimics the fold geometry itself, indicating that these contours were also folded in a sheath-like manner. We propose that this sheath-like pattern is the result of a two-stage process

that reflects a change of the mode of nappe formation in the subduction zone from thrusting to fold nappe formation. First, thrusting of a hot oceanic nappe onto a colder continental nappe created an inverted peak-thermal gradient. Second, sheath folding of this composite nappe structure together with the previously established peak-temperature pattern during exhumation. This pattern was preserved because temperatures decreased during retrograde exhumation metamorphism and remained less than the subduction-related peak temperatures during the later Barrovian overprint. The fold ascended with diapir-like kinematics in the subduction channel.

1 | INTRODUCTION

Mountain building in subduction–collision zones is typically characterized by two distinct modes of plate convergence. First, oceanic lithosphere is consumed during subduction which eventually leads in a second stage to continental collision after complete closure of the ocean. The transition from subduction to collision is accompanied by a rearrangement of crustal deformation patterns and the thermal structure of the involved lithosphere. Temperature (T) controls several key parameters, for example, rock strength, metamorphic reactions and fluid flow, which are all critical for the dynamics of orogens and subduction zones. These parameters, on the other hand, feed back to the temperature distribution and thermal budget (e.g. Goffé et al., 2003). However, direct observation of any transient thermal state and its dynamics on the large scale is not possible and studies on this topic have to use either indirect observations with geophysical methods or numerical simulations. Both approaches are strongly dependent on boundary conditions and other assumptions and therefore require comparison with natural examples. These data are obtained by reconstructing the thermal state of tectonic units exhumed from subduction zones and now accessible at the surface. Many studies have either explored the thermal evolution of subducted units with time (e.g. classical geochronological studies; Steck & Hunziker, 1994) or the thermal structure integrated over a certain timespan (e.g. Wiederkehr et al., 2011), but combining both aspects to reconstruct the evolution of the thermal structure, possibly in three dimensions, remains very challenging (Luth & Willingshofer, 2008).

In the Alps, a classical area to study processes related to the subduction-collision transition, many tectonic units experienced Alpine pressure- (P-) dominated subduction-zone metamorphism. In the Western Alps, several studies revealed the geometry of orogen-scale, subduction-related metamorphic structures (e.g. Agard et al., 2002; Babist et al., 2006; Beltrando et al., 2010; Bousquet et al., 2008). In other regions of the Alps, however, the subduction-related thermal imprint has been obscured by a second, later thermal event and most studies focussed on reconstructing the thermal structure of this Barrovian metamorphism (e.g. Cliff et al., 1985; Droop, 1985; Hoernes & Friedrichsen, 1974; Scharf, Handy, Favaro, et al., 2013). This is particularly the case for many of the Penninic and Sub-Penninic units in the Lepontine Dome and the Tauern Window, where the nappe boundaries are crosscut by Barrovian isograds (Oberhänsli et al., 2004). The thermal structure of the regional, collision-related Barrovian metamorphism is overprinted by late collision-related deformation structures. For example, large-scale folds in the Tauern Window (e.g. Hoinkes et al., 1999) and backfolds in the Lepontine Dome deformed post-nappe isograds (e.g. Steck & Hunziker, 1994). Moreover, external fold-and-thrust belts are generally characterized by large-scale cylindricity of thrust nappes and along-strike continuity of metamorphic isograds (e.g. Bousquet et al., 2008; Frey et al., 1999). For instance, the pattern of peak-metamorphic temperatures in the Helvetic nappes was passively folded when the Aiguilles Rouges and Aar massifs were uplifted along basement thrusts (Girault et al., 2020).

Like the cylindrical Jura and Helvetic external belts, some Penninic and Sub-Penninic nappes of the Central and Western Alps that formed during subduction and exhumation occur along the strike of the orogen, suggesting that they were originally also cylindrical. Polyphase post-nappe refolding, however, resulted in generally non-cylindrical nappe geometries (e.g. Maxelon & Mancktelow, 2005; Milnes, 1974; Steck et al., 2019). Given the spatial coincidence of thermal and deformational structure in collisional settings, the question arises if a similar relationship exists in the non-cylindrical (fold) nappes that formed in subduction settings. In other words, do non-cylindrical (fold) nappes also exhibit a non-cylindrical thermal structure that in some way corresponds with the nappe geometry?

We attempt to answer this question by investigating a highly non-cylindrical fold nappe in the Tauern Window

TABLE 1 Regional deformation phases in the Tauern Window after Schmid et al. (2013)

Phase	Events
D1	Early subduction of Alpine Tethys
D2	Late subduction of Alpine Tethys, HP metamorphism in Glockner and Rote Wand nappes
D3	Exhumation, Formation of Seidlwinkl sheath fold
D4	Accretion of European margin, Formation of Venediger Duplex
D5	Indentation, doming in the Tauern Window

in three dimensions. We show that even for a multi-phase metamorphic evolution, the thermal structure of the earlier, subduction-related event can be partly reconstructed. We apply Raman spectroscopy on carbonaceous matter (CM) to yield metamorphic peak-T. The pattern of peak-T corresponds well with the originally non-cylindrical geometry of the Seidlwinkl fold nappe. Additionally, the results show how the subduction-related peak-T distribution is overprinted by the post-exhumation Barrovian metamorphism that was most intense in the European basement of the Eastern Alps.

2 | GEOLOGICAL OVERVIEW AND THERMAL HISTORY OF THE TAUERN WINDOW

The Tauern Window is the largest tectonic window in the Alps, exposing units that display a polyphase metamorphic history with older P-dominated and younger T-dominated Alpine metamorphism (e.g. Droop, 1985; Hoernes & Friedrichsen, 1974; Hoinkes et al., 1999; Oberhänsli et al., 2004). This change from P- to T-dominated overprints reflects the large-scale Alpine evolution from a subduction- to a collision-dominated orogenesis. The Tauern Window itself formed mainly in Neogene times during relatively late stages of continental collision by a combination of crustal-scale indentation, doming and lateral escape (e.g. Ratschbacher et al., 1991; Rosenberg et al., 2007; Scharf, Handy, Favaro, et al., 2013; Schmid et al., 2013). Normal faulting at the eastern and western ends of the window together with erosional denudation in response to doming removed the Austroalpine lid (Favaro et al., 2017) and led to the emergence of the underlying Penninic and Sub-Penninic nappes. These nappes witnessed intense metamorphism and deformation during earlier Palaeogene subduction and collision.

The Austroalpine nappes, as the uppermost tectonic units surrounding the Tauern Window, comprise a nappe stack formed during the Cretaceous Eoalpine orogeny along the Adriatic continental margin (e.g. Froitzheim et al., 1994; Schmid et al., 2004). Below this Eoalpine nappe stack are thrust sheets of oceanic lithosphere that were derived from the Alpine Tethys (also called the Penninic Ocean; e.g., Kurz et al., 1996, 1998; Schmid et al., 2004), as well as thrust sheets of the distal European continental margin (Kurz et al., 2008), termed Penninic and Sub-Penninic nappes respectively. Following the nomenclature of Schmid et al. (2013), the Penninic nappes can be subdivided into the Matrei Zone (upper, older, Piemont–Liguria part) and the Glockner nappe system (lower, younger, Valais part). The Sub-Penninic nappes comprise, from top to bottom, the Modereck nappe system—in the central Tauern Window composed of the Rote Wand Nappe (above) and Trögereck Nappe (below)—the Eclogite Zone and the Venediger nappe system.

The Alpine Tethys separated the European and Adriatic continents in Jurassic and Cretaceous times but was consumed during Palaeogene southward subduction (e.g. Handy et al., 2010; Stampfli & Borel, 2004). Early and late subduction-related structures correspond, respectively, to the regional deformation phases D1 and D2 in the tectonic scheme of Schmid et al. (2013), which we adopt in the following (Table 1). During subduction, some of the Penninic and Sub-Penninic nappes were subjected to high-P (HP) metamorphism (i.e. Glockner Nappe s.str., Rote Wand Nappe, Trögereck Nappe, Eclogite Zone) and intense deformation which involved the formation of a crustal-scale sheath fold nappe (D3) now exposed in the central Tauern Window (Seidlwinkl sheath fold, Groß et al., 2020). During the onset of the collisional stage of Alpine orogeny, the more proximal European continental margin was progressively accreted below the Alpine nappe stack (D4), forming the Venediger nappe system (Schmid et al., 2013). The Venediger nappe system is exposed in two structural subdomes, the eastern and western Tauern subdomes (ETD and WTD respectively; Figure 1). The subdomes are separated by an axial depression, the central Tauern depression (CTD). All units were affected by a Barrow-type, high-T (HT) metamorphic event in late Oligocene time (e.g. Cliff et al., 1985; Favaro et al., 2015; Höck, 1980) that was overprinted by orogen-parallel extensional shearing and doming (D5; e.g., Favaro et al., 2015; Scharf et al., 2016).
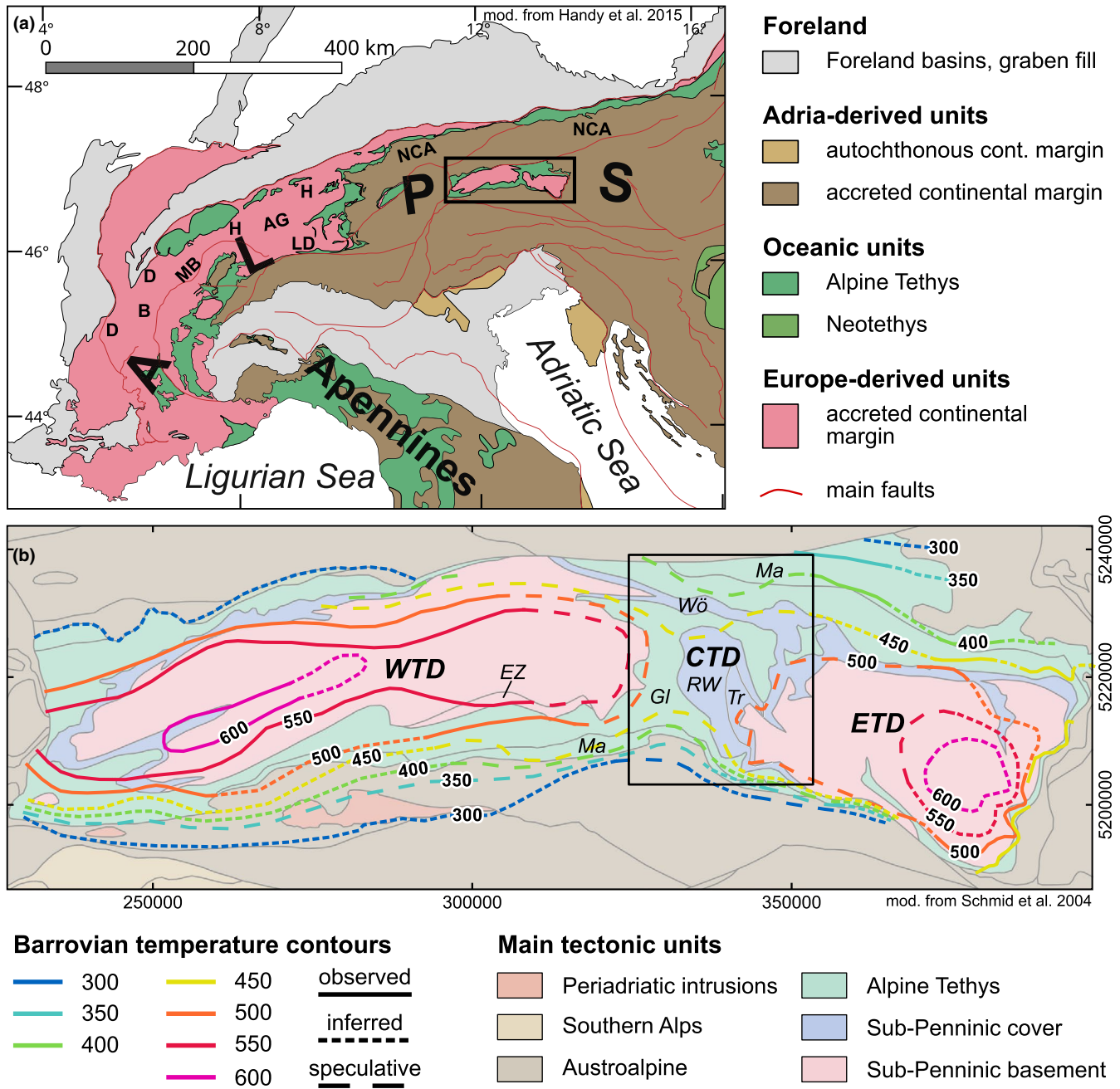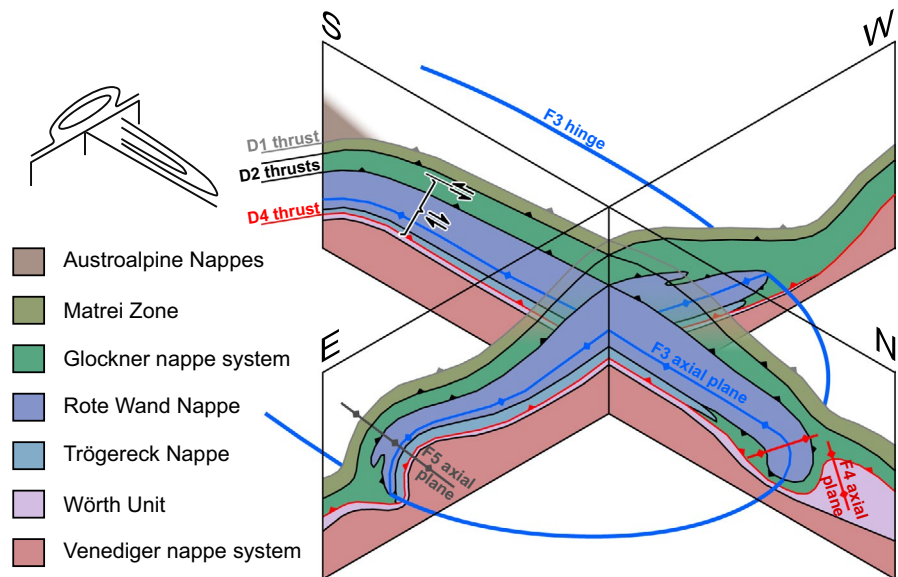
FIGURE 1 (a) Tectonic overview map of the Alps (modified from Handy et al., 2015). Black rectangle denotes the location of map in (b). AG = Aar and Gotthard massifs, B = Belledonne Massif, D = Dauphinois Zone, H = Helvetic nappes, LD = Lepontine Dome, MB = Mont-Blanc Massif, NCA = Northern Calcareous Alps. (b) Tectonic map of the Tauern Window region (modified from Schmid et al., 2004) and peak-*T* contours of regional metamorphism compiled from Bousquet et al. (2012), Dachs (1990), Droop (1985), Hoernes and Friedrichsen (1974), Rosenberg et al. (2018)—WTD; Favaro et al. (2015), Inger and Cliff (1994), Lambert (1970), Oxburgh et al. (1966), Reddy et al. (1993), Scharf, et al. (2013)—ETD; Frank et al. (1987), own data—CTD. The contours mainly reflect peak conditions of Barrovian 'Tauernkristallisation' metamorphism. The black rectangle delineates the main research area and the location of the Seidlwinkl sheath fold (Figure 2). EZ = Eclogite Zone, Wö = Wörth Unit, Tr = Trögereck Nappe, RW = Rote Wand Nappe, Gl = Glockner nappe system, Ma = Matrei Zone (includes the 'Nordrahmenzone'). Details on the compilation of peak-*T* contours are given in Appendix S1

2.1 | The Seidlwinkl sheath fold in the central Tauern Window

Recent studies document the existence of a crustal-scale, recumbent and isoclinal sheath fold nappe in the central part of the Tauern Window, called the Seidlwinkl sheath fold (Figure 2; Groß et al., 2020). This fold is a composite structure comprising the folded thrust contact of the oceanic Glockner Nappe s.str. with the underlying continental Rote Wand Nappe (D2). During D3, the Glockner Nappe s.str. was

wrapped around the Rote Wand Nappe, both units together forming a fold nappe that, also during D3, was thrust over the parautochthonous cover of the Venediger nappe system (Wörth Unit in the ETD, Figure 1). The axis of this fold nappe curves almost 180° which results in a sheath fold geometry. The fold formed at HP conditions in the Alpine subduction zone and was exhumed partly in an extrusion channel between opposite-sense shear zones—a normal fault above and a thrust below (Groß et al., 2020). Continued shortening during D4 led to the accretion of the Sub-Penninic nappes below the Seidlwinkl sheath fold and the formation of the Wörth antiform north of the sheath fold (Figure 1).

Sheath folds on the metre to sub-metre scale are common in all kinds of shear zones around the world (e.g. Alsop et al., 2007). However, sheath folds as large as the one discussed here—that is, on the scale of hundreds of metres to several kilometres—are only rarely described, despite the fact that sufficiently large shear zones that could exhibit such structures are fairly common. Very large sheath folds are usually associated with orogenic crustal flow of high-grade and highly deformed basement (e.g. Bonamici et al., 2011; Chetty et al., 2012; Goscombe, 1991; Henderson, 1981; Vollmer, 1988) and only few have been described from a subduction-exhumation setting (e.g. Lacassin & Mattauer, 1985; Searle & Alsop, 2007), as in this study.

The tectonic units with European affinity discussed here have a common lithostratigraphy, which generally begins with pre-Variscan basement intruded by late-Variscan plutons and overlain unconformably by post-Variscan—mostly Mesozoic—clastic sediments and carbonates (e.g. Kurz et al., 1998; Schmid et al., 2013). This sequence is especially well developed in the Rote Wand Nappe, which forms the core of the Seidlwinkl sheath fold (Frasl & Frank, 1964; Kurz et al., 1998; Pestal & Hellerschmidt-Alber, 2011). This allows

a reconstruction of the fold geometry using well-defined stratigraphic marker horizons. The oceanic units discussed below comprise mafic and ultramafic basement and abundant carbonate-bearing marine sediments of Jurassic and/or Cretaceous age (Höck et al., 2006; Koller & Pestal, 2003; Lemoine, 2003; Reitz et al., 1990).

2.2 | Peak *P–T*- and timing-estimates for Barrovian metamorphism

A Barrow-type HT metamorphic event termed 'Tauernkristallisation' (Sander, 1911) overprinted the Alpine nappe stack in and around the Tauern Window to variable degrees (Hoinkes et al., 1999) in Oligocene time (*c.* 30–27 Ma; Christensen et al., 1994; Cliff et al., 1985; Favaro et al., 2015). This event also largely overprinted the older HP assemblages (e.g. Kurz et al., 2008). The large-scale distribution of peak-T conditions of the Barrovian event in the Tauern Window have been mapped in and around the western (Dachs, 1990; Hoernes & Friedrichsen, 1974) and eastern Tauern subdomes (Cliff et al., 1985; Scharf, Handy, Favaro, et al., 2013) and its conditions have been quantified by a variety of thermometrical methods (e.g. oxygen isotope fractionation, calcite–dolomite equilibrium, Raman spectroscopy on carbonaceous material). They all confirmed the concentric Barrovian temperature pattern around the two subdomes of the Tauern Window. The highest peak-T at amphibolite facies conditions (>600°C and 0.7 GPa) were reached in the central, structurally lowest parts of the western and eastern Tauern domes. From there, the peak-T radially decrease to values of greenschist facies conditions at the perimeter of the window and even lower conditions in Austroalpine units outside of the window. However, so far

there are only few data in the CTD (Bickle & Powell, 1977; Dachs & Proyer, 2001; Frank et al., 1987) and the interpretation of these data is ambiguous because of overlapping metamorphic conditions of the Barrovian and subduction-related events (see below). Therefore, the continuation of isotherms of Barrovian metamorphism across the depression between the subdomes, as shown in previous compilations (Bousquet et al., 2012), is speculative. We compiled a new map of existing and own data of peak-*T* for the Barrovian event in the Tauern Window (Figure 1) with focus on the central Tauern depression. Details of this compilation are given in Appendix S1. This compilation confirms the large-scale concentric thermal structure of the isotherms of Barrovian metamorphism, but shows that the high-grade isograds related to this event in the subdomes are separated from each other by a zone of lower Barrovian peak-T in the central Tauern depression.

2.3 | Peak pressure–temperature and estimates of timing for subduction metamorphism

Alpine subduction in the Tauern Window is evidenced by the occurrence of HP mineral parageneses in metabasites and metasediments with Mesozoic protolith ages. This HP event reached pressure conditions that indicate deep subduction to sub-crustal depths in tectonic units derived from the Alpine Tethys (Glockner Nappe s.str.) and the distal European margin (Rote Wand Nappe, Trögereck Nappe, Eclogite Zone). Several *P–T* estimates for these units exist, ranging from ~2.0 to 2.3 GPa and 600°C in the continent-derived Eclogite Zone (Dachs, 1986, 1990; Frank et al., 1987; Hoschek, 2001; Kurz et al., 1998; Stöckhert et al., 1997; Zimmermann et al., 1994) to ~1.7 GPa and 570°C in the oceanic Glockner Nappe s.str. (Dachs & Proyer, 2001). For the latter unit, Groß et al. (2020) determined somewhat higher peak pressures of up to 2.3 GPa. Recent studies have also confirmed the widespread existence of this HP event (2 GPa, 500°C) in the continental Rote Wand and Trögereck nappes (belonging to the Modereck nappe system) in the central Tauern Window (Groß et al., 2020; Schmidt, 2015). For the uppermost Penninic nappe unit, the Matrei Zone, Koller and Pestal (2003) estimated conditions of subduction metamorphism to be ~0.9–1.0 GPa and 360–370°C. For the Sub-Penninic Venediger nappe system, peak pressures of ~1.0 GPa at ~500°C were reported (Droop, 1985; Selverstone, 1993; Selverstone et al., 1984). The tectonic units with a HP imprint experienced variable degrees of HT overprint during regional Barrovian metamorphism, depending on the locality. Previous mapping of peak-*T* concentrated on the western and eastern Tauern subdomes to either side of the HP units mostly exposed in the central Tauern depression. Therefore, the thermal imprint of the

subduction-related metamorphism has not yet been mapped as well as the Barrovian event, although in the Central Alps, it has been shown that at least parts of subduction-related peak-*T* patterns escaped later thermal overprint (e.g. Wiederkehr et al., 2011).

The age of the baric peak of subduction metamorphism is in debate. Studies that used Ar–Ar dating on phengite and hornblende found upper Eocene ages for peak-P conditions: *c.* 39 Ma for the Rote Wand nappe (Kurz et al., 2008) and 45–38 Ma for the Eclogite Zone (Kurz et al., 2008; Ratschbacher et al., 2004). Abundant younger Ar–Ar ages in the range 36–32 Ma for the same units and the Glockner Nappe s.str. are commonly interpreted as cooling or deformation ages set during syn-deformational retrogression from peak-P conditions (Kurz et al., 2008; Zimmermann et al., 1994). On the other hand, dating with high-retentivity isotopic systems using allanite (U–Pb, Smye et al., 2011) and garnet (Lu–Hf, Nagel et al., 2013) yielded similarly young ages of *c.* 35–33 Ma for the prograde path and subsequent baric peak for metabasites of the Eclogite Zone and associated metasediments.

3 | RAMAN SPECTROSCOPY ON CARBONACEOUS MATERIAL

Raman spectra of carbonaceous matter (RSCM) show two main intensity bands in the regions 1,000–1,500 cm^{-1} and 1,500–1,700 cm^{-1}, commonly named D- and G-band respectively. Ideally, the G-band is the only band of perfectly ordered graphite in the first-order region (~1,100 to 1,800 cm^{-1}), whereas the various D-bands are the result of double-resonant Raman scattering induced by disorder in the graphite crystal lattice (Reich & Thomsen, 2004). The relative intensities of these bands therefore depend on the crystallization state of the CM. The degree of ordering in the graphite crystal lattice gradually increases with increasing metamorphic temperature. Since the graphitization process of CM is irreversible, the temperatures obtained reflect the thermal peak of the whole metamorphic history of the investigated specimen (Beyssac et al., 2002). Several calibrations for this geothermometer have been proposed so far (e.g. Aoya et al., 2010; Beyssac et al., 2002; Kouketsu et al., 2014; Lahfid et al., 2010; Lünsdorf et al., 2017). These calibrations differ somewhat in terms of absolute temperatures derived from measuring the crystallization state of CM. However, the relative temperature differences between samples—the information used in this study—is well-resolved irrespective of the calibration used. We chose the calibration of Lünsdorf et al. (2017) because it has the advantage of being applicable to a wide range of metamorphic temperatures (160–600°C). Furthermore, their method provides a well-integrated automatic spectrum-fitting approach realized by their IFORS

software that eliminates operator bias during curve fitting (Lünsdorf et al., 2017). Their method uses a statistical parameter ('scaled total area' = STA) that has been calibrated against the known metamorphic peak-T of a large number of reference samples.

Spectra of non-surface exposed CM particles in polished thin sections were obtained on a Horiba ISA Dilor Labram micro-confocal Raman spectrometer with a Nd-YAG laser (532.15 nm wavelength, 300 mm focal length) and a grating with 1,800 grooves/mm. A high spatial resolution (~1 μm spot size) was achieved by using a 400 μm wide confocal hole, a slit width of 100 μm and a 100× objective. The spectrometer was centred at 1,100 or 1,200 cm^{-1} to ensure sufficiently large background signal on both sides of the CM-band region. The acquisition time was 20 s with two accumulations. In order to avoid thermal destruction or photo-bleaching of the CM, the laser power was attenuated with a 0.3 filter to 2–3 mW of laser energy on the sample. In each sample we measured ~30 individual CM particles, preferentially as inclusions in transparent or translucent host phases (quartz, white mica, garnet, chloritoid, calcite, chlorite), in order to avoid alteration caused by sample preparation. All spectra were fitted automatically with the IFORS software in the range of 1,000–1,900 cm^{-1} (= first-order region of CM bands). Peaks and background were modelled simultaneously, with pseudo-Voigt functions for the peaks and a fifth-order polynomial as baseline correction. The results were manually checked for integrity (no spurious peaks, convergence of multiple runs, no strong fluorescence) so that those fittings with insufficient quality could be discarded from further evaluation. A temperature was calculated for each remaining spectrum by using the Lünsdorf et al. (2017) calibration, resulting in a range of temperatures for each sample. For graphical evaluation, the results of each sample are plotted in a diagram that shows the individual temperature measurements (Figure 3). The mean of this temperature range is assumed to represent the 'true' sample temperature (e.g. Beyssac et al., 2002), with its uncertainty given by the 95% confidence interval (CI)

of the mean. The within-sample heterogeneity is expressed as one standard deviation (1σ) of all temperature values obtained in the sample. Additionally, it is visualized with a kernel density estimate (KDE; Figure 3), making it easy to perceive non-unimodal or strongly skewed temperature distributions. The absolute geological uncertainty of each temperature estimate (compared with other methods, e.g., thermodynamic modelling) is in the order of ~30°C (Aoya et al., 2010).

3.1 | Robustness of the RSCM-temperature estimates regarding amount of analyses

Aoya et al. (2010) suggested that at least 25–30 individual measurements are required for each sample to assure that the scatter of the average of a statistical value (their R2 ratio) reduces to a narrow and reasonable range. In order to investigate the robustness of our temperature estimates, we expanded their approach by applying a simple bootstrapping analysis. For this purpose, we measured 60 CM grains in one specimen (PG25; 47.06106°N 12.79165°E), which is twice the number of 30 CM grains usually measured. This large sample data set is randomly resampled (with replacement) to generate synthetic subsamples of variable size, n (3–60 CM grains; number of analyses per sample = n). This procedure is repeated for 150 iterations. In each iteration, the most important statistical parameters (mean, median, standard deviation, confidence interval) are calculated. After all iterations, the scatter of these values is evaluated as a KDE for each n and the results are plotted (Figure 4).

With increasing number of analyses per sample n, the scatter of mean, median and SD strongly decreases until it stays nearly constant within a narrow range for n greater than ~20–25. The scatter of the confidence interval and its absolute value steadily decrease with increasing n, but the latter becomes reasonably low (<10°C) at n of ~25–30. Given the overall uncertainty of the method, 30 analysed CM particles per sample is therefore sufficient to obtain precise, robust and

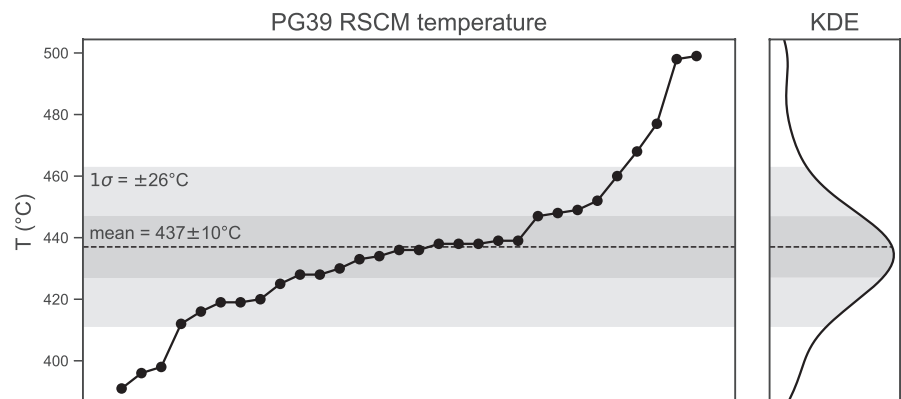**FIGURE 3** Exemplary summary of all RSCM-temperature estimates from sample PG39. Individual measurements are on the *x*-axis. Sample mean (stippled line), 95% CI (dark shaded area) and one standard deviation (light shaded area) are also shown
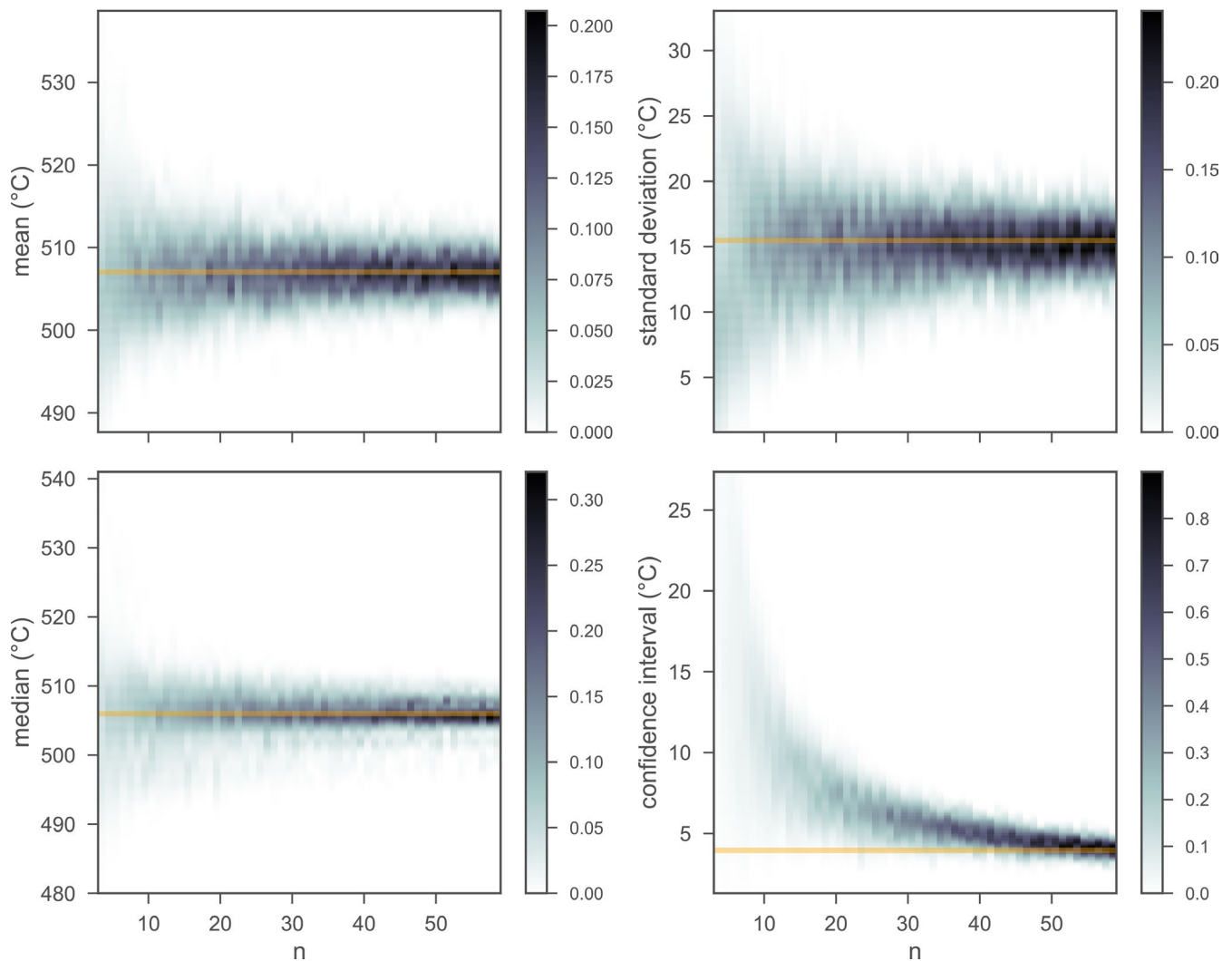
Convergence of statistical parameters with increasing n, 150 iterations

FIGURE 4 Bootstrapping analysis for increasing n shows that statistical parameters largely converge to sample average values (orange horizontal lines, calculated with actual data from sample PG25) for *n* of 3–60. The grey scale denotes the kernel density

reproducible results. The RSCM raw data, result from spectrum fitting with IFORS and the resulting RSCM-temperature data are available in the GFZ Data Services repository (Groß et al., 2020).

4 | RESULTS

The results of RSCM-temperature analyses of all 104 samples are summarized in Table 2 and shown on a map (Figure 5) and several cross-sections (Figure 6) of the study area. A map with sample locations (Figure S2) and enlarged, high-resolution versions of the RSCM map (Figure S3) and cross-sections (Figure S5) are provided in the Supporting Information. For details on cross-section construction and data projection, we refer to the Appendix S2 and Figure S1. Our new peak-*T* data are in good agreement with the temperature estimates obtained

by Frank et al. (1987) that are also shown on the map and cross-sections.

The highest temperatures of ~520°C were obtained near the contact of the Rote Wand Nappe with the Glockner Nappe s.str. in the southern central part of the study area (Figures 5 and 6). From there, temperatures decrease in all directions except south, that is, towards the 'root' of the fold nappe. The lowest temperature estimates of ~350–400°C are located along the northern border of the Tauern Window. For the lithologies with post-Variscan stratigraphic ages used in this study, peak-*T* was reached either during Alpine subduction or later regional Barrow-type thermal overprint (Tauernkristallisation). The relative uncertainty of the temperature estimates is generally on the order of ±10°C or even less, which is very low and facilitates resolution of even small temperature differences between samples.

TABLE 2 Results of RSCM-temperature analyses. Sample coordinates are in decimal degrees. n = number of analysed spectra per sample; CI = 95% confidence interval of the mean; 1σ = 1 standard deviation; Q1, Q3 = first and third quartile respectively

Sample	Sample coordinates		n	Mean (°C)	CI (°C)	1σ (°C)	Q1 (°C)	Median (°C)	Q3 (°C)	Min (°C)	Max (°C)
	Lat	Lon									
F15/17	47.09157	12.94475	27	491	10	26	482	497	508	426	544
PG13	47.06887	12.83963	30	521	10	26	508	516	534	475	582
PG18	47.06476	12.86976	32	507	9	25	500	508	524	420	543
PG21	47.08413	12.74363	43	488	8	27	468	482	504	439	544
PG25	47.06106	12.79165	60	507	4	15	496	506	512	478	550
PG29	47.08102	12.90041	31	471	8	22	452	468	478	440	528
PG32	47.08144	12.91461	37	498	7	20	484	498	511	462	565
PG39	47.20519	12.85492	30	437	10	26	421	436	448	391	499
PG41	47.17778	12.81980	31	436	11	29	417	431	448	383	516
PG48	47.08263	12.83997	31	521	8	21	506	519	534	488	565
PG50	47.08252	12.83879	31	513	8	21	498	512	528	465	555
PG59	47.08215	12.83455	33	554	9	25	546	560	570	468	581
PG60	47.08210	12.83445	30	522	10	26	505	522	542	470	560
PG61	47.08153	12.85327	40	505	6	20	490	506	520	462	550
PG70	47.01313	12.92355	31	489	5	15	482	489	500	456	519
PG89	46.99970	12.92027	32	518	9	24	503	522	536	456	577
PG93	47.00327	12.91583	33	500	6	17	491	503	515	462	524
PG102	47.02236	12.92846	35	503	9	26	493	505	518	428	559
PG117	47.08595	12.87196	31	493	5	13	485	494	500	469	522
PG119	47.01313	12.92362	27	479	5	13	469	475	484	460	511
PG126	47.02228	12.93056	32	474	5	13	468	472	479	448	509
PG130	47.11207	12.82534	30	485	8	21	474	487	498	441	538
PG133	47.08307	12.74402	34	508	9	27	492	511	523	444	561
PG139	47.13251	12.84119	30	497	6	17	487	496	507	461	537
PG141	47.13907	12.84402	28	496	10	27	483	496	513	447	557
PG143	47.12378	12.81980	31	486	10	28	471	480	500	442	558
PG144	47.13876	12.80937	31	488	8	23	474	488	508	436	527
PG145	47.19293	12.82843	29	447	16	43	411	428	489	393	523
PG150	47.16490	12.90585	30	481	7	20	467	480	497	447	517
PG155	47.12797	12.96785	30	485	10	28	462	479	504	441	541
PG157	47.18769	12.94088	31	478	11	30	454	477	501	410	527
PG159	47.18671	12.93966	32	492	9	26	474	500	513	437	523
PG161	47.11427	12.92652	31	484	7	20	467	488	495	444	524
PG163	47.10725	12.91453	30	493	7	19	482	488	497	471	552
PG167	47.11128	12.92077	30	478	9	24	462	474	492	430	539
PG176	47.21406	12.94204	29	456	9	23	438	450	463	426	507
PG178	47.19469	12.97066	31	486	7	20	475	487	501	439	523
PG180	47.19993	12.97218	33	486	9	25	468	491	507	434	518
PG182	47.21032	12.96617	30	427	11	28	416	432	440	337	490
PG185	47.20305	12.96998	30	466	12	31	435	469	487	408	520
PG188	47.23495	12.99888	36	390	11	33	368	377	418	339	480
PG189	47.23056	13.00392	33	463	10	28	439	465	484	419	505

(Continues)

TABLE 2 (Continued)

Sample	Sample coordinates		*n*	Mean (°C)	CI (°C)	1σ (°C)	Q1 (°C)	Median (°C)	Q3 (°C)	Min (°C)	Max (°C)
	Lat	Lon									
PG190	47.27203	12.97922	32	374	10	27	360	372	380	335	468
PG192	47.27418	12.97755	30	347	9	25	336	344	353	301	415
PG194	47.20717	12.96765	30	453	10	27	436	450	469	386	509
PG195	47.20255	12.96635	35	467	10	28	449	463	492	420	537
PG206	47.19690	12.85223	30	470	13	36	452	468	496	390	535
PG208	47.08437	12.87841	29	482	9	24	465	482	505	442	524
PG214	47.01109	12.86035	22	508	13	29	489	509	527	431	555
PG216	47.01108	12.85454	23	441	5	11	437	440	448	418	471
PG220	47.06841	12.81982	25	472	8	20	463	469	477	411	514
PG223	47.16329	12.83337	29	489	6	16	482	492	500	454	522
PG228	47.16800	12.85818	30	485	6	15	478	488	492	451	528
PG229	47.16596	12.84674	22	490	7	17	480	488	496	465	529
PG233	47.15095	12.85413	30	464	11	28	452	462	476	379	521
PG235	47.09259	12.81526	22	503	7	16	493	498	508	468	534
PG238	47.09688	12.80421	30	519	7	18	507	520	530	486	552
PG242	47.18543	12.84582	29	489	7	17	479	491	498	452	522
PG243	47.18949	12.84968	27	467	11	27	450	458	496	424	509
PG247	47.19540	12.85067	28	472	16	40	442	465	514	393	530
PG250	47.21473	12.83527	32	442	9	26	427	436	451	393	502
PG251	47.17596	12.85750	30	492	6	15	479	490	504	466	517
PG254	47.17878	12.85954	30	494	8	22	479	497	508	429	532
PG256	47.18293	12.86215	29	455	8	21	440	452	469	408	516
PG258	47.18758	12.86514	29	487	12	30	469	489	506	433	541
PG260	47.12132	12.87562	32	482	8	23	469	475	498	434	538
PG261	47.11988	12.86785	30	491	10	27	481	493	506	414	534
PG262	47.10316	12.85082	29	498	14	37	488	504	521	371	560
PG264	47.09594	12.85090	21	481	11	25	466	478	494	427	551
PG267	47.16742	12.72921	30	507	6	16	500	506	515	479	541
PG268	47.16865	12.73390	31	465	9	25	452	465	472	410	522
PG270	47.16470	12.73638	30	487	10	27	472	491	503	433	541
PG275	47.25731	12.74228	29	427	8	21	419	427	437	379	468
PG277	47.14867	12.99552	31	487	7	19	476	492	502	436	509
PG278	47.14360	13.00195	30	475	7	19	462	476	484	438	526
PG280	47.13720	13.01402	22	498	10	22	481	500	517	454	530
PG282	47.13592	12.99925	29	478	12	30	453	475	494	424	541
PG283	47.03030	12.85314	23	502	8	19	490	498	518	464	537
PG285	47.06587	12.76461	30	510	7	19	494	511	524	478	549
PG288	47.06203	12.76904	41	524	11	36	497	515	553	464	585
PG291	47.22328	12.82085	31	440	10	26	422	440	456	394	504
PG293	47.23642	12.83177	27	397	8	20	386	401	410	350	432
PG295	47.14147	12.77297	30	500	6	16	486	498	514	476	533
PG299	47.13174	12.75609	30	512	6	16	499	512	521	489	552
PG301	47.15023	12.79487	30	488	10	27	466	485	506	443	544

(Continues)

TABLE 2 (Continued)

Sample	Sample coordinates		n	Mean (°C)	CI (°C)	1σ (°C)	Q1 (°C)	Median (°C)	Q3 (°C)	Min (°C)	Max (°C)
	Lat	Lon									
PG302	47.11424	12.79357	32	496	7	19	483	498	507	460	530
PG303	47.10947	12.78826	30	491	6	16	478	494	501	462	522
PG304	47.10638	12.78808	30	508	8	20	496	511	523	462	543
PG305	47.11280	12.79372	31	504	10	29	494	505	518	397	579
PG334	47.17431	12.79483	28	481	9	23	468	478	497	437	534
PG335	47.16805	12.78938	26	496	7	18	480	494	511	469	526
PG336	47.17211	12.80316	30	475	10	27	458	468	497	433	533
PG337	47.17139	12.80800	27	444	14	36	426	434	454	384	519
PG338	47.05176	12.76148	30	399	7	18	388	395	411	371	444
PG340	47.05461	12.76606	28	420	6	16	412	420	428	392	469
YD003	47.04476	12.81100	27	506	7	18	493	507	522	463	535
YD005	47.04457	12.80834	28	471	12	32	452	479	494	386	530
YD006	47.04480	12.80639	28	461	11	29	442	455	480	407	535
YD007	47.04478	12.80628	27	501	9	23	488	502	518	435	541
YD010	47.04185	12.80246	28	446	8	19	437	440	456	402	511
YD011	47.03905	12.79922	29	414	17	44	403	417	437	281	490
YD012	47.03737	12.79731	30	388	9	23	371	382	398	360	437
YD014	47.03385	12.79360	28	410	12	32	393	410	427	306	487
YD017	47.03938	12.80034	28	409	10	25	393	406	423	370	475

4.1 | 3D temperature distribution in the central Tauern Window in map view and cross-sections

Both normal and inverted peak-temperature gradients exist in the cross-sections (Figure 6), that is, trends in peak-T that increase both upwards and downwards. Gradual and more abrupt, fault-related transitions between these two modes also occur. Going upsection from the core of the Venediger basement where peak-T in excess of 550°C is documented (Figure 5; e.g., Hoernes & Friedrichsen, 1974; Scharf, Handy, Ziemann, et al., 2013), we observe that temperatures first decrease to ~480°C in the inverted lower limb of the Seidlwinkl sheath fold. Upsection from there, RSCM temperature increases again to ~520°C along the contact between Glockner and Rote Wand nappes in the upper limb of the central part of the sheath fold. Further upsection towards the hanging-wall of the Seidlwinkl sheath fold, RSCM temperature drops from 520 to ~410°C over a distance of only several hundred metres. East and west from the centre of the Seidlwinkl fold, towards the western and eastern Tauern domes, the temperature inversion cannot be resolved unambiguously, either due to a lack of exposure of the Glockner and Rote Wand nappes or because it does not exist. North of the sheath fold, an inversion in the temperature gradient occurs at the contact of the Sub-Penninic Wörth Unit and the tectonically higher,

Penninic Rauris Nappe, that is, in the upper limb of the Wörth Antiform.

5 | DISCUSSION

5.1 | Kinetic and deformational effects on the RSCM thermometer

Kinetic and deformational effects were reported to potentially influence the RSCM thermometer. In cases that involve little deformation of the rocks containing CM, such as contact metamorphic settings, it has been shown that the graphitization process reaches steady state within several hundreds of years (Mori et al., 2015, 2017). This implies that on geological time-scales, temperature is the main factor controlling the degree of graphitization of CM and kinetic effects are negligible. Kirilova et al. (2018) reported that brittle deformation decreases the degree of graphitization in CM by mechanical destruction of the crystal lattice. We avoided this effect by only analysing small isolated CM particles included in other mineral phases and clearly not affected by any brittle structures. On the other hand, by comparing the crystallinity of large undeformed CM flakes with CM aggregates in the schistosity of a nearby shear zone, Barzoi (2015) showed that ductile strain can potentially increase the degree of
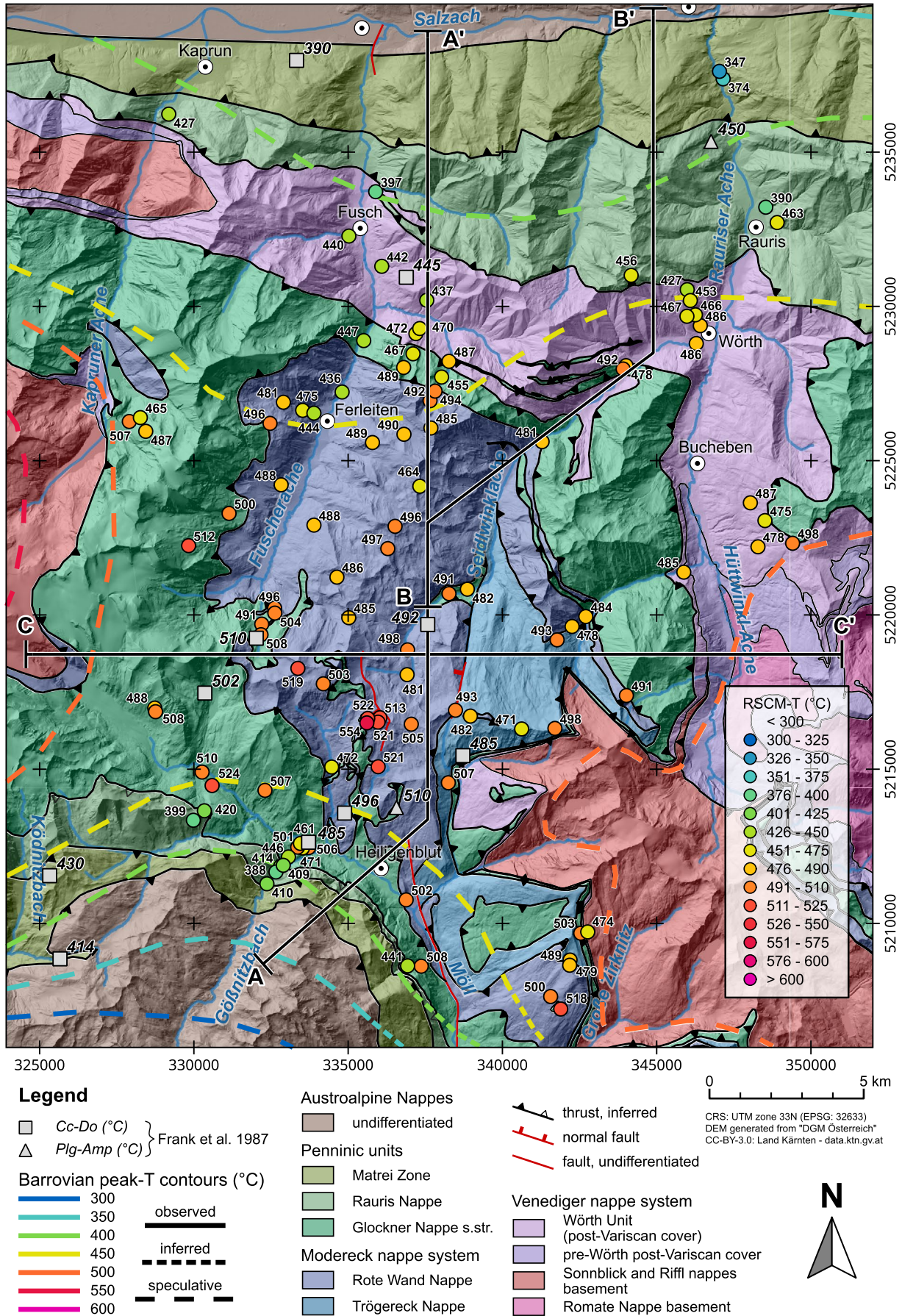
FIGURE 5 RSCM peak-temperature map of the central Tauern Window. Peak-*T* contours are displayed for the Barrovian metamorphic stage. A high-resolution version of this figure is available in Figure S3
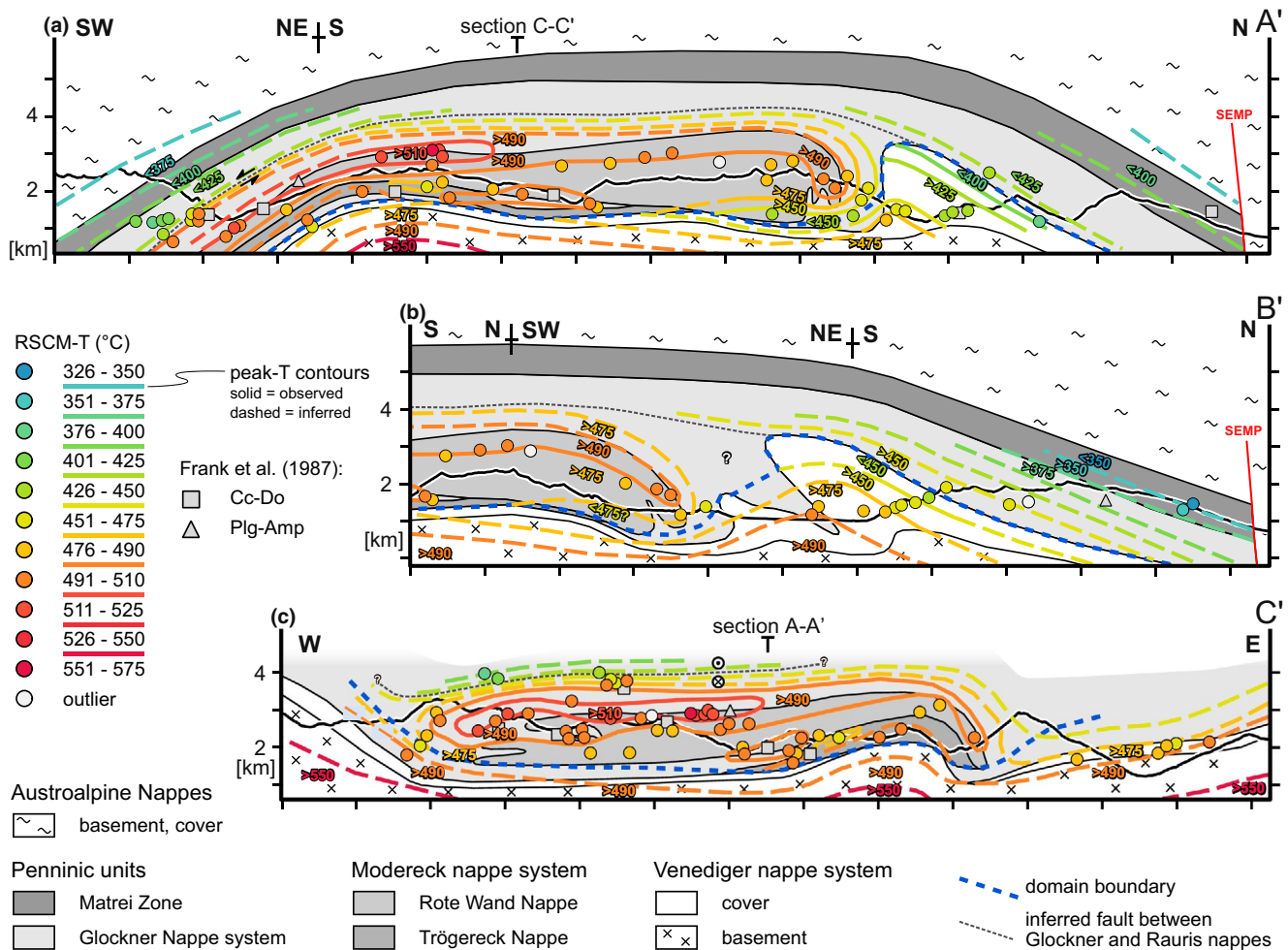
FIGURE 6 Profiles with RSCM temperatures of the central Tauern Window. Contours in these profiles are peak-*T* contours of both Barrovian and subduction-related metamorphic stages. See Figure 5 for traces of the section. A high-resolution version of this figure is available in Figure S5

graphitization in CM. Several observations indicate that such an effect did not substantially influence our results. First, we only measured unoriented CM inclusions and avoided CM aligned in shear zones or shear bands. Second, our results are well in line with other estimates on the peak-*T* conditions obtained with alternative methods (see above). Third, we observe a steady upward decrease of RSCM temperatures across the high-strain shear zone between the Glockner s.str. and Rauris nappes. This indicates that the degree of graphitization was not significantly affected by strain. Therefore, we see no evidence for any kinetic effects on our results.

5.2 | Distinguishing peak-*T* domains of subduction-related and Barrow-related metamorphism

Radiometric dating and thermobarometry (e.g. Dachs & Proyer, 2001; Kurz et al., 2008) show that the tectonic units in the Seidlwinkl sheath fold experienced a two-stage

metamorphic evolution that is typical for subduction-collision orogens. In the map and cross-sections (Figures 5 and 6), we distinguish parts of the Seidlwinkl sheath fold that still preserve subduction-related peak-*T* conditions from those where the peak-*T* are of the overprinting Barrovian metamorphism.

Discriminating between the subduction-related and the Barrovian metamorphic events in the central Tauern Window using thermometric data only is not easy. Both events reached very similar peak-*T* conditions of ~400 to 550°C in different parts of the fold. Additionally, the peak-*T* pattern not only reflects the overprinting relationship of these two metamorphic events but was also substantially modified by D5 deformation. RSCM data cannot discriminate between different metamorphic events in a single rock sample, since due to its irreversibility it yields peak-*T* only; in this sense it contrasts with geothermobarometry applied to multiple generations of minerals or mineral assemblages and their overprinting fabric relationships. In Figure 7, we sketch some potential overprinting patterns used in our interpretation of the RSCM data from the central Tauern Window. Note that unusual features, for
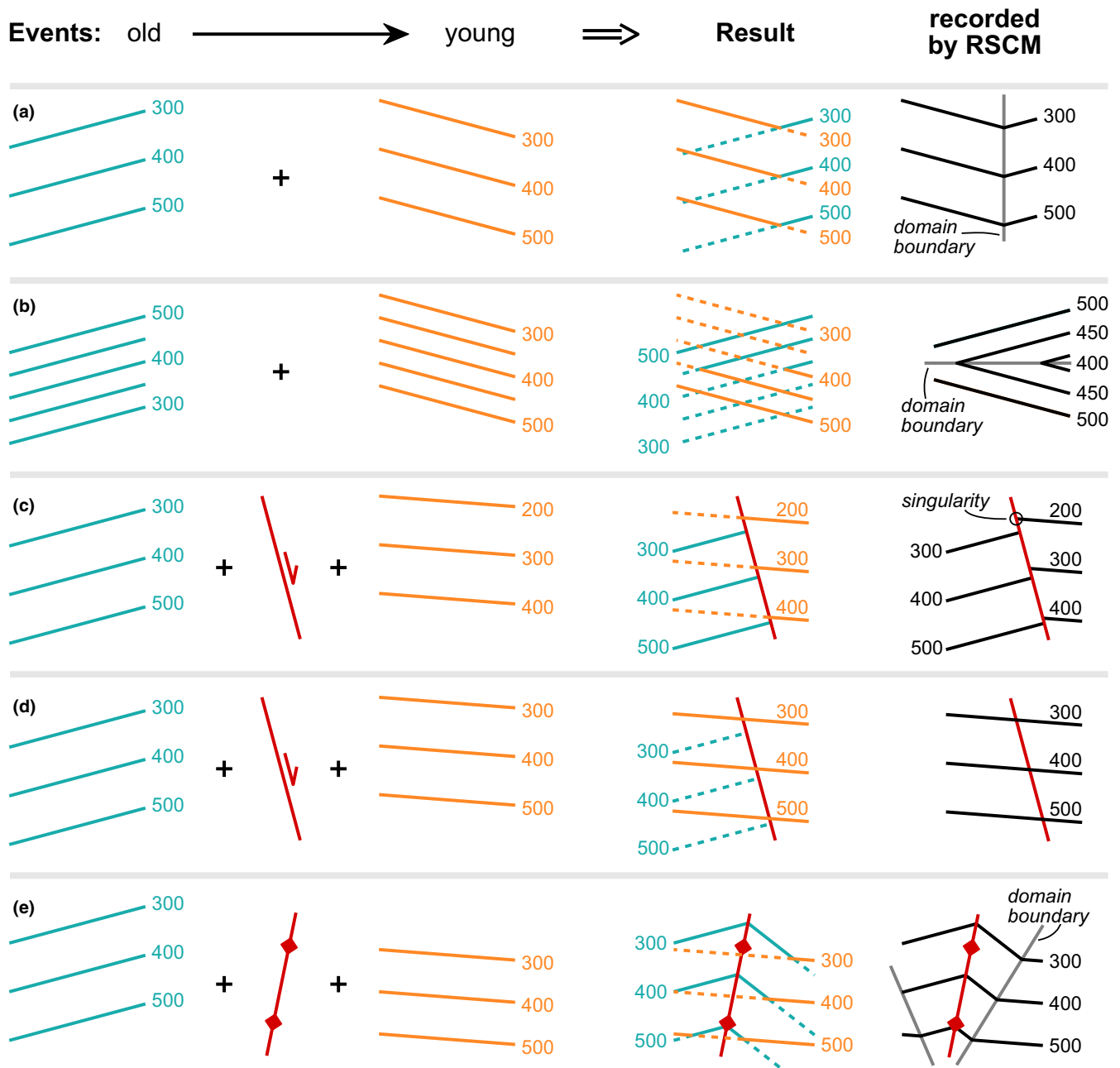
FIGURE 7 Hypothetical patterns of overlapping isotherms of two metamorphic stages and the associated peak-T contour patterns recorded by RSCM thermometry. (a) inclined T-fields of two metamorphic events are only partly recorded by RSCM thermometry; (b) inverted T-field partly overprinted by a normal-sense T-field. Inversion of apparent gradient in the RSCM-temperature pattern indicates boundary between old and young domain; (c) combination of metamorphism and faulting can lead to singularities in the RSCM-temperature pattern; (d) as in (c) but with more intense second metamorphic stage that erases the record of earlier stages; (e) combination of two-phase metamorphism and folding

example, discontinuous or kinked iso-peak temperature lines (singularities), may occur in RSCM-temperature patterns (Figure 7b,c). These features reflect the irreversibility of the graphitization process. During a single metamorphic event, peak-T may have been reached diachronously, for example, due to conductive heat flow from hotter to colder parts of the fold. Therefore, we refer to the isolines of peak-T as recorded by RSCM not as geotherms but as peak-T contours.

We base our distinction between subduction-related and Barrovian RSCM-temperature patterns on the following reasoning: The Barrovian event is younger than the subduction-related event, as proven by radiometric dating (e.g. Favaro et al., 2015; Zimmermann et al., 1994) and overprinting relationships (e.g. Dachs & Proyer, 2001). It is characterized by peak-T conditions that decrease with increasing distance from the cores of the western and eastern Tauren

subdomes (Figure 1; e.g., Hoernes & Friedrichsen, 1974; Scharf, Handy, Favaro, et al., 2013). We attribute inversions of this normal metamorphic gradient in the nappe stack to the inheritance of an older metamorphic event that was not overprinted by the Barrovian event (schematically shown in Figure 7b). Such an inversion occurs in the central Tauern Window in the lower limb of the Seidlwinkl sheath fold and at the base of the Rauris Nappe in the northern part of the study area (Figure 6). Therefore, we consider the RSCM temperature in the units below this inversion to reflect the peak-*T* during the Tauernkristallisation; the RSCM temperatures in the units above the inversion reflect the subduction-related peak-*T* pattern. Using this approach, we are able to define a metamorphic domain boundary between those areas of the central Tauern Window that were affected by the Barrovian overprint of the RSCM peak-T and those that still preserve the original subduction-related thermal peak conditions.

We projected RSCM-temperature estimates into cross-sections (Figure 6) to construct peak-*T* contours highlighting the lateral and vertical variations in peak-*T*. Interpolating isolines involved some generalization of the RSCM results and the assumption that peak-*T* increased towards the cores of the WTD and ETD.

Very few temperature estimates had to be excluded from interpretation, mainly where their projection from the map into the cross-section, for example, due to strong non-cylindricity of the folds (Figure S1) led to outliers in the temperature pattern. However, we regard the first-order geometry and features of both peak-*T* domains summarized in Figure 8 as sufficiently robust for further interpretation.

5.3 | Thermal structure of the Barrovian peak-T domain

Over most of the study area, the Barrovian peak-*T* pattern is not observed in the RSCM data, since the older subduction-related peak-*T* were higher and their pattern is still preserved and exposed at the surface. An exception is the Wörth Unit (Figure 6). Large portions of the rocks belonging to this unit (mostly graphite-rich pelitic phyllites) are amassed in the Wörth Antiform, immediately north of the Seidlwinkl sheath fold (W. Frank, pers. comm August 2017; Groß et al., 2020). In the Wörth Unit, the peak-*T* clearly decreases upwards, with peak values of ~490–500°C (SE of Bucheben village, Figures 5 and 8b) in the stratigraphically lowest part of the sedimentary cover sequence, close to the eastern Tauern subdome, where the Wörth Unit directly overlies the basement of the Venediger nappe system. Peak-*T* gradually decreases northward and upsection to ~430°C in the upper (northern) limb of the Wörth Antiform, directly at the contact of the Wörth Unit with the overlying Rauris Nappe. Where rocks above the metamorphic domain boundary are exposed at the surface, reconstruction of the Barrovian peak-*T* pattern relies on indirect evidence: The observed RSCM peak-T in the structurally lowest parts of the sheath fold provide an upper bound on the conditions reached during the Tauernkristallisation. In the central and northeastern part of the fold, the maximum estimate for the Barrovian temperature is ~480°C as obtained on samples from the upper and lower Seidlwinkl Valley (Figure 5). At the base of the northwestern part of the sheath fold, exposed in the Fuscher Valley (near Ferleiten, Figure 5), the Barrovian peak-*T* is ~440°C or less. At the southern border of the central Tauern Window

FIGURE 8 Sketch of the peak-*T* pattern in the Seidlwinkl sheath fold. The sections are parallel (a) and perpendicular (b) to the nappe transport direction. The boundary between subduction- and Barrow-related peak-*T* domains (dashed black line) is marked by inversion of the peak-*T* gradient. In the Barrovian domain, peak-*T* decreases away from the core of the basement domes. In the subduction domain, peak-*T* contours form a sheath-like pattern similar to the lithological layering

near the town of Heiligenblut (Figure 5), where the Penninic nappes dip southwestward below the Austroalpine nappes, the RSCM data constrain the peak-*T* of Barrovian metamorphism to ~400°C.

These observations are in line with the concentric pattern of Barrovian isograds in the Tauern Window (e.g. Hoinkes et al., 1999). Similar to the western and eastern Tauern subdomes, the metamorphic peak temperatures in the central Tauern depression decrease north- and southwards, nearly perpendicular to the east–west trend of the window. However, the structural depression in the central Tauern area coincides with a pronounced negative anomaly in the peak-*T* pattern. This is reflected by inwards-bending of lower-grade peak-*T* contours (<~450°C) in the central Tauern depression, whereas higher-grade peak-*T* contours (>~500°C) of the eastern and western Tauern domes do not connect across the depression. The peak-*T* contours are oblique to the main thrusts (e.g. D2 thrust fault between Glockner Nappe s.str. and Rote Wand Nappe) and large-scale D3 and D4 fold axes (e.g. fold axis of D4 Wörth Antiform) in the central Tauern depression. This indicates that the dominant structural imprint in this area pre-dates the peak of the Barrovian 'Tauernkristallisation' metamorphism. This is in line with independent microstructural observations (Figure 9), for example from the Wörth antiform, where the axial plane foliation defined by a prominent crenulation is overgrown by post-kinematic (post-D4) albite porphyroblasts, indicating heating after D4.
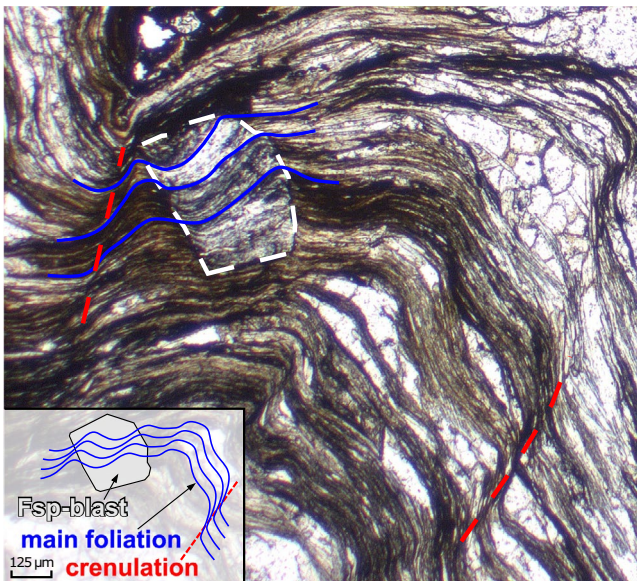

FIGURE 9 Post-kinematic feldspar porphyroblast in sample PG247 (47.19540°N 12.85067°E) overgrowing the axial plane foliation (i.e. crenulation) of the D4 Wörth antiform. The main foliation that is crenulated is the regional S3

5.4 | Thermal structure of the subduction-related peak-T domain

The metamorphic domain boundary between peak temperatures of the subduction-related and Barrovian domains is marked by an inversion in the direction of peak-*T* decrease (Figures 6 and 8). South of the Wörth Antiform, this inversion is located approximately in the lower limb of the Seidlwinkl sheath fold. In the northern limb of the Wörth Antiform, it is located at the base of the Rauris Nappe. There, peak-*T* decreases northward and upsection from ~460 to 350°C, although details like the inclination of the peak-*T* contours cannot be resolved due to low sample coverage. The peak-*T* contours close to the northern margin of the central Tauern Window are more or less continuous with the iso-temperature contours reported for the western and eastern Tauern subdomes (Frank et al., 1987; Hoernes & Friedrichsen, 1974) that are thought to represent peak-*T* conditions of the Barrovian metamorphism Scharf, Handy, Favaro, et al. (2013). Therefore, the boundary between the subduction-related and the younger Barrow-related domain is poorly defined in the northernmost part of the central Tauern Window.

In the E–W cross-section (Figures 6 and 8b) south of the Wörth Antiform, peak-*T* contours have an eye-shaped pattern in the inner part of the sheath fold and an omega-shaped pattern in its periphery. This pattern is well resolved in the west but somewhat speculative in the east due to lower sample coverage. In the N–S cross-sections (Figures 6 and 8a), the peak-*T* contours are also curved and display a pattern very similar to the folded lithological layering. In essence, the high-grade peak-*T* contours in the Seidlwinkl sheath fold display a sheath-like pattern. This pattern is subparallel to the lithological layering that defines the sheath fold itself. However, the highest RSCM temperatures cluster along the D2 thrust boundary between the Glockner nappe s.str. and Rote Wand nappe.

In the south, towards the top of the Seidlwinkl sheath fold, the peak-*T* contours converge so that the 410 and 510°C contours are only ~1 km apart. This steep peak-T gradient of ~100°C/km indicates post-peak-*T* tectonic thinning. This zone of thinning coincides with the nappe contact between the Glockner nappe s.str. and overlying Rauris nappe; it is a major D3 normal fault that partly accommodated the exhumation of the HP units in its footwall relative to the low-*P* units in its hangingwall (Groß et al., 2020). The observation of narrowly spaced peak-*T* contours near the proposed contact is further independent evidence of this normal fault.

5.5 | Formation of sheath-like peak-temperature pattern in the Alpine subduction zone

In an active subduction zone, the isotherm pattern is shaped by the rate of subduction, the temperature difference

between the upper and lower plates bounding the zone, the length of the zone boundaries and by the characteristic heat diffusion length of rocks making up the subduction zone itself (Peacock, 1996). This pattern, schematically shown in Figure 10a, may be disturbed by varied thermal parameters of subducted rocks (e.g. Goffé et al., 2003) or when rock units start to move relative to its surroundings, for example, when crustal nappes are sheared off from the downgoing slab and start to move relative to each other (Figure 10b). This was the case for D2 thrusting of the Glockner Nappe s.str. onto the Rote Wand Nappe and subsequent extrusion of the composite Rote Wand-Glockner s.str. Nappe during D3 (Groß et al., 2020). However, the peak-T contours are not necessarily isotherms that were 'frozen in' at the moment when rocks in the Seidlwinkl fold began to ascend; individual RSCM temperatures are snapshots of the peak temperature when a rock started to cool. Rocks metamorphosed in settings dynamically changing from subduction to collision typically follow P–T–time paths where the temperature peak follows the maximum burial (highest P)

with some delay (e.g. England & Thompson, 1984). P–T paths from the Rote Wand and Glockner s.str. nappes have shapes indicating that peak-T was reached after only a small decrease of pressure from maximum burial conditions and that further decompression was concomitant with slightly decreasing temperatures (Dachs & Proyer, 2001; Groß et al., 2020; Kurz et al., 2008). This suggests that during their exhumation, the Glockner s.str. and Rote Wand nappes were initially heated but then, during most of exhumation, cooled so that the peak-T contours behaved as passive markers during deformation.

The preservation of the highest peak temperatures in the Seidlwinkl fold along the boundary between the Glockner s.str. and Rote Wand nappes can be explained by D2 thrusting of the former nappe onto the latter, assuming that upon attaining maximum depth immediately before D2, the Glockner Nappe s.str. was deeper and reached a higher peak-T than the Rote Wand Nappe.

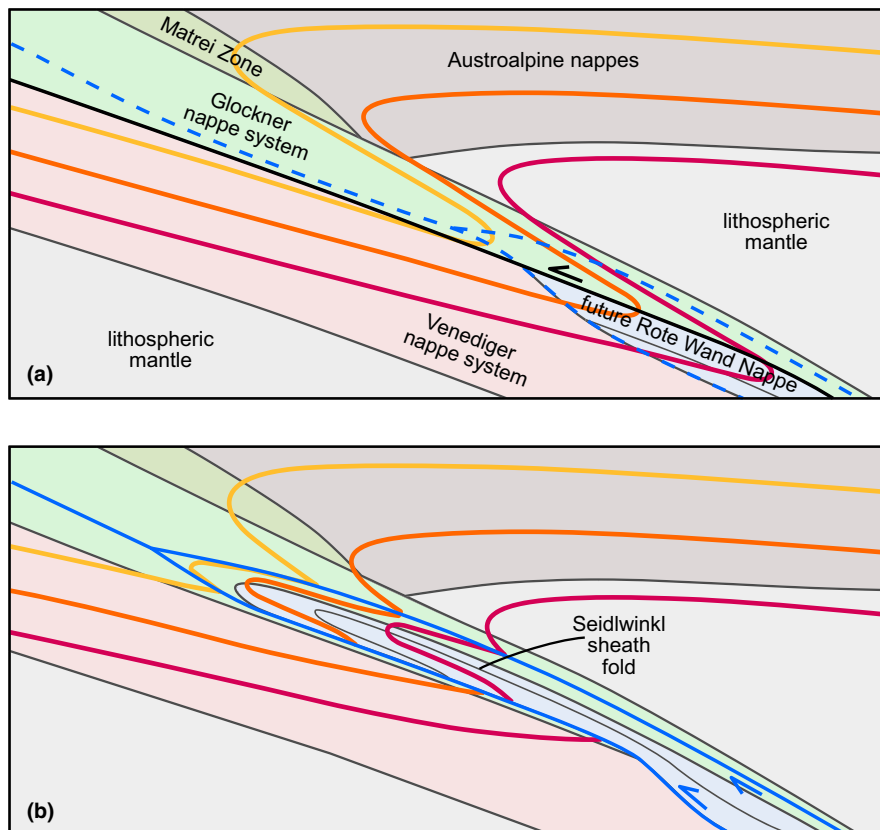Another interpretation of the observed peak-T pattern is that it resulted from shear heating along the D2 thrust, that

FIGURE 10 Schematic development of folded peak-T contours (red, orange and yellow lines) by formation of a sheath fold nappe during exhumation; inspired by Escher and Beaumont (1997). Before exhumation (a), isotherms in the subduction zone largely correspond to peak-T contours that are recorded by CM in the subducted rocks. These are largely subparallel to the lithological layering. With the onset of exhumation, the units start to cool and peak-T contours are preserved by CM. These lines act as markers that are passively deformed together with the folding rock. Further deformation during exhumation in an extrusion channel (b) leads to (sheath-) fold nappe formation and shearing of lithological markers and peak-T contours, resulting in a fold pattern that mimics that of the folded units. In the non-exhuming material, peak-T contours are constantly reset as peak-T increases in response to heat diffusion and advection

is, the generation of heat due to viscous strain that caused a temperature rise (e.g. Molnar & England, 1990).

However, these two mechanisms, which are not mutually exclusive, cannot explain the decrease in peak-T to the east and west along the thrust plane, that is, towards the hinges of the Seidlwinkl Fold. Instead, the geometry of folded peak-T contours is similar to that of the D3 sheath fold pattern outlined by the lithological contacts, including the D2 thrust between the Glockner s.str. and Rote Wand nappes. This suggests that either the rocks within the Seidlwinkl sheath fold cooled below their peak-T between the D2 and D3 stages so that D3 folding of the contours was strictly passive, or that D3 started at temperatures close to the thermal peak and involved heat transported advectively by the exhuming Seidlwinkl fold. In that case, the D3 strain rates must have been high enough to maintain thermal disequilibrium, thus preventing smoothing of the contours due to heat loss (England & Molnar, 1993). In any case, the shear strain during D3 folding and mylonitic shearing was sufficiently high to rotate the initially oblique lithological contacts and peak-T contours into near-parallelism. In contrast, peak-T contours folded in shallower parts of an orogen are typically highly oblique to the lithological and nappe boundaries (e.g. Girault et al., 2020; Wiederkehr et al., 2011).

Classically, sheath folds are regarded to form by passive amplification of curved fold hinges in homogeneous simple shear (Cobbold & Quinquis, 1980). Domal structures on a surface subparallel to the shear plane will amplify into sheath folds that close in the direction of shear. Conversely, sheath folds closing in the opposite direction will form from depressions in the surface (Fossen & Rykkelid, 1990). Additionally, it has been shown that sheath folds also form by flow perturbation around weak (e.g. Exner & Dabrowski, 2010; Reber et al., 2012) or strong (e.g. Adamuszek & Dabrowski, 2017; Marques & Cobbold, 1995) inclusions in overall simple shear. While the initial geometry of the Rote Wand Nappe may have formed a domal perturbation in the D3 top-to-the-foreland shear zone (Groß et al., 2020), the peak-T contours show an inverted temperature gradient throughout the Rote Wand nappe and any downward bulge in the contour pattern before shearing would have been transformed into a sheath fold closing opposite to the northward D3 shear direction. This is why in the light of our new thermometric data we favour strain variations perpendicular to the direction of transport (Alsop & Holdsworth, 2007; Xypolias & Alsop, 2014) as an alternative mechanism for the formation of the Seidlwinkl sheath fold. In sections through the fold that are close to the X–Z plane of D3 finite strain (Figures 6 and 8a), such variations exist between the top-to-the-south normal-sense shear zone along the top of the Glockner nappe s.str. and the top-to-the-north shear zone below. In the section perpendicular to the transport direction (Figures 6 and 8b), the eye- and omega-shaped patterns of the peak-T contours can be explained by D3 top-to-the-north

strain decreasing sideways from a maximum in the centre of the fold. In this interpretation, the D3 exhumation of the Glockner s.str. and Rote Wand nappes in the Seidlwinkl fold was diapiric in the purely kinematic sense of a tubular rock body that rises with respect to its wall rocks and that closes upwards in the direction of material flow (see also Kossak-Glowczewski et al., 2017). Unlike a classical pluton or salt diapir, however, the Seidlwinkl fold moved along bounding faults without disturbing the tectonostratigraphy of the surrounding rocks, that is, as a pip-like extruding body (Wheeler et al., 2001).

Our observations are in line with a perturbation of the flow field in the subduction–exhumation zone with enhanced top-to-the-foreland flow in the core of the Seidlwinkl sheath fold. According to analogue and numerical models, flow perturbations may be caused by rheological heterogeneities in shear zones (Adamuszek & Dabrowski, 2017; Exner & Dabrowski, 2010; Marques & Cobbold, 1995; Reber et al., 2012). Such heterogeneities may well have been inherited along distal parts of continental passive margins where the continental crust is strongly segmented by normal faults (e.g. Boillot et al., 1989) and varies in composition and thickness. Therefore, Groß et al. (2020) proposed that the Seidlwinkl fold originates from a promontory or extensional allochthon of the distal European margin that reached into the Alpine Tethys. If subducted, such isolated continental segments may provide first-order rheological and structural perturbations in the subduction channel where sheath folds can nucleate. We speculate that further amplification of the sheath fold happened at temperatures high enough to keep the viscosity contrast between different lithological layers <10 which is the upper limit for sheath folding in analogue experiments (Marques et al., 2008). Strain localized in highly attenuated limbs of the exhuming fold nappe, while the hot ascending core preserved relics of HP assemblages from deeper parts of the subduction channel. So although D3 shearing affected the entire fold, its localization in the fold limbs with opposite-sense shearing (top-N thrusting in the footwall and top-S normal shearing in the footwall) enabled exhumation to shallower depths with a temperature of ≤400°C. At that final stage, more proximal, less segmented parts of the European margin with more uniform thickness were underthrust below the Seidlwinkl sheath fold (Venediger nappe system) and the Wörth antiform developed in front of the Seidlwinkl sheath fold. This D4 deformation was highly cylindrical, indicating that during D4, lateral variations in the flow field had diminished and given way to more uniform flow. This style of deformation may be characteristic for more external and shallower parts of an orogen.

Sheath fold formation is not a feature unique to deep parts of orogens or subduction channels (e.g. Alsop et al., 2007). However, large (i.e. nappe-scale) sheath folds require both a large initial perturbation and a shear zone that is even wider

than the perturbation. Subduction of distal continental margins provides both ingredients for the formation of large sheath folds; a wide, high-strain shear zone in the subduction channel and structural-rheological perturbations in the form of subducted extensional allochthons and continental ribbons. As is suggested from the folded pattern of peak-*T*emperature contours in the Seidlwinkl sheath fold, the formation of such large sheath folds can also partly involve diapir-like flow perturbations in an overall simple-shear dominated shear zone.

6 | SUMMARY AND CONCLUSIONS

The distribution of peak-metamorphic temperatures in the central Tauern Window is consistent with a thermal history marked by two metamorphic events, each leaving behind a distinct peak-*T* pattern.

1. The younger event is the regional-scale, collision-related Barrovian metamorphic event known as Tauernkristallisation, characterized by a normal-sense geothermal gradient (i.e. upward-decreasing temperature) and peak-*T* decreasing away from the cores of the large subdomes towards the central depression and the surroundings of the Window.

2. The older metamorphic stage is related to Palaeogene subduction. The area where the temperature pattern of this older event is still preserved corresponds with the areal extent of the Seidlwinkl sheath fold, an isoclinal and highly non-cylindrical fold nappe related to subduction and exhumation prior to collisional nappe stacking and Barrovian metamorphism. The peak-*T* contours of subduction-related metamorphism are folded and their geometry mimics that of the fold itself. The peak-*T* pattern is characterized by an inverted peak-thermal gradient in the fold's inverted lower limb and a normal gradient in the fold's upper limb. Peak-*T* contours close towards the northern, western and eastern parts of the fold, similar to lithological marker horizons marking the fold itself.

3. Narrowly spaced peak-*T* contours (100°C drop over 1 km) at the top of the Seidlwinkl sheath fold are interpreted as independent evidence for the recently proposed substantial normal-sense offset within the Glockner nappe system (Groß et al., 2020).

4. We propose that the sheath-like pattern of peak-*T* contours is the result of a change in the mode of nappe formation. During a first stage (Figure 10a), the hotter oceanic Glockner Nappe s.str. was thrust onto the colder continental Rote Wand Nappe. During the second stage (Figure 10b), the Rote Wand Nappe was then detached from the downgoing European lithosphere. Together with the overlying Glockner Nappe s.str., it started to exhume, cool and form a composite sheath fold nappe—the Seidlwinkl Fold. During this process, parts of the Glockner Nappe s.str. were wrapped around the Rote Wand Nappe. The previously established peak-*T* contours were deformed during exhumation and sheath folding. This second mode of nappe formation involving nappe folding is characterized by pervasive deformation of the whole fold nappe.

5. The sheath-like peak-*T* pattern can be explained by formation of the sheath fold as a diapir-like structure that formed during its ascent in the subduction channel. Such a diapir-like flow pattern requires lateral strain gradients, with the greatest amount of finite strain localized in the fold limbs with opposite-sense shear zones, and the greatest amount of exhumation in the centre of the sheath fold.

ORCID

Philip Groß https://orcid.org/0000-0002-5766-169X
Mark R. Handy https://orcid.org/0000-0001-5923-9751
Timm John https://orcid.org/0000-0003-0686-5585

REFERENCES

Adamuszek, M., & Dabrowski, M. (2017). Sheath folds as a strain gauge in simple shear. *Journal of Structural Geology*, *102*, 21–36. https://doi.org/10.1016/j.jsg.2017.06.008

Agard, P., Monié, P., Jolivet, L., & Goffé, B. (2002). Exhumation of the Schistes Lustrés complex: In situ laser probe 40Ar/39Ar constraints and implications for the Western Alps. *Journal of Metamorphic Geology*, *20*(6), 599–618.

Alsop, G. I., & Holdsworth, R. E. (2007). Flow perturbation folding in shear zones. *Geological Society, London, Special Publications*, *272*(1), 75–101. https://doi.org/10.1144/GSL.SP.2007.272.01.06

Alsop, G. I., Holdsworth, R. E., & McCaffrey, K. J. W. (2007). Scale invariant sheath folds in salt, sediments and shear zones. *Journal of*

Structural Geology, *29*(10), 1585–1604. https://doi.org/10.1016/j.jsg.2007.07.012

Aoya, M., Kouketsu, Y., Endo, S., Shimizu, H., Mizukami, T., Nakamura, D., & Wallis, S. (2010). Extending the applicability of the Raman carbonaceous-material geothermometer using data from contact metamorphic rocks. *Journal of Metamorphic Geology*, *28*(9), 895–914. https://doi.org/10.1111/j.1525-1314.2010.00896.x

Babist, J., Handy, M. R., Konrad-Schmolke, M., & Hammerschmidt, K. (2006). Precollisional, multistage exhumation of subducted continental crust: The Sesia Zone, western Alps. *Tectonics*, *25*(6). https://doi.org/10.1029/2005TC001927

Barzoi, S. C. (2015). Shear stress in the graphitization of carbonaceous matter during the low-grade metamorphism from the northern Parang Mountains (South Carpathians)—Implications to graphite geothermometry. *International Journal of Coal Geology*, *146*, 179–187. https://doi.org/10.1016/j.coal.2015.05.008

Beltrando, M., Rubatto, D., & Manatschal, G. (2010). From passive margins to orogens: The link between ocean-continent transition zones and (ultra) high-pressure metamorphism. *Geology*, *38*(6), 559–562. https://doi.org/10.1130/G30768.1

Beyssac, O., Goffé, B., Chopin, C., & Rouzaud, J. N. (2002). Raman spectra of carbonaceous material in metasediments: A new geothermometer. *Journal of Metamorphic Geology*, *20*(9), 859–871. https://doi.org/10.1046/j.1525-1314.2002.00408.x

Bickle, M. J., & Powell, R. (1977). Calcite-dolomite geothermometry for iron-bearing carbonates. *Contributions to Mineralogy and Petrology*, *59*(3), 281–292. https://doi.org/10.1007/BF00374557

Boillot, G., Mougenot, D., Girardeau, J., & Winterer, E. L. (1989). Rifting processes on the West Galicia Margin, Spain. Chapter 23: European-African Margins.

Bonamici, C. E., Tikoff, B., & Goodwin, L. B. (2011). Anatomy of a 10 km scale sheath fold, Mount Hay ridge, Arunta Region, central Australia: The structural record of deep crustal flow. *Tectonics*, *30*(6). TC6015. https://orcid.org/10.1029/2011TC002873

Bousquet, R., Oberhänsli, R., Goffé, B., Wiederkehr, M., Koller, F., Schmid, S. M., Schuster, R., Engi, M., Berger, A., & Martinotti, G. (2008). Metamorphism of metasediments at the scale of an orogen: A key to the Tertiary geodynamic evolution of the Alps. *Geological Society, London, Special Publications*, *298*(1), 393–411. https://doi.org/10.1144/SP298.18

Bousquet, R., Oberhänsli, R., Schmid, S. M., Berger, A., Wiederkehr, M., Robert, C. … Zeilinger, G. (2012). Metamorphic framework of the Alps: CCGM/CGMW.

Chetty, T. R. K., Yellappa, T., Mohanty, D. P., Nagesh, P., Sivappa, V. V., Santosh, M., & Tsunogae, T. (2012). Mega sheath fold of the Mahadevi hills, Cauvery Suture Zone, southern India: Implication for accretionary tectonics. *Journal of the Geological Society of India*, *80*(6), 747–758. https://doi.org/10.1007/s12594-012-0205-x

Christensen, J. N., Selverstone, J., Rosenfeld, J. L., & DePaolo, D. J. (1994). Correlation by Rb-Sr geochronology of garnet growth histories from different structural levels within the Tauern Window, Eastern Alps. *Contributions to Mineralogy and Petrology*, *118*(1), 1–12. https://doi.org/10.1007/BF00310607

Cliff, R. A., Droop, G. T. R., & Rex, D. C. (1985). Alpine metamorphism in the south-east Tauern Window, Austria: 2. Rates of heating, cooling and uplift. *Journal of Metamorphic Geology*, *3*(4), 403–415. https://doi.org/10.1111/j.1525-1314.1985.tb00327.x

Cobbold, P. R., & Quinquis, H. (1980). Development of sheath folds in shear regimes. *Journal of Structural Geology*, *2*(1), 119–126. https://doi.org/10.1016/0191-8141(80)90041-3

Dachs, E. (1986). High-pressure mineral assemblages and their breakdown-products in metasediments South of the Grossvenediger, Tauern Window, Austria. *Schweizerische Mineralogische Und Petrographische Mitteilungen*, *66*(1–2), 145–161.

Dachs, E. (1990). Geothermobarometry in metasediments of the southern Grossvenediger area (Tauern Window, Austria). *Journal of Metamorphic Geology*, *8*(2), 217–230. https://doi.org/10.1111/j.1525-1314.1990.tb00467.x

Dachs, E., & Proyer, A. (2001). Relics of high-pressure metamorphism from the Grossglockner region, Hohe Tauern, Austria. *European Journal of Mineralogy*, *13*(1), 67–86.

Droop, G. T. R. (1985). Alpine metamorphism in the south-east Tauern Window, Austria: 1. P-T variations in space and time. *Journal of Metamorphic Geology*, *3*(4), 371–402. https://doi.org/10.1111/j.1525-1314.1985.tb00326.x

England, P. C., & Molnar, P. (1993). The interpretation of inverted metamorphic isograds using simple physical calculations. *Tectonics*, *12*(1), 145–157. https://doi.org/10.1029/92TC00850

England, P. C., & Thompson, A. B. (1984). Pressure—temperature—time paths of regional metamorphism I. Heat transfer during the evolution of regions of thickened continental crust. *Journal of Petrology*, *25*(4), 894–928.

Escher, A., & Beaumont, C. (1997). Formation, burial and exhumation of basement nappes at crustal scale: A geometric model based on the Western Swiss-Italian Alps. *Journal of Structural Geology*, *19*(7), 955–974. https://doi.org/10.1016/S0191-8141(97)00022-9

Exner, U., & Dabrowski, M. (2010). Monoclinic and triclinic 3D flanking structures around elliptical cracks. *Journal of Structural Geology*, *32*(12), 2009–2021. https://doi.org/10.1016/j.jsg.2010.08.002

Favaro, S., Handy, M. R., Scharf, A., & Schuster, R. (2017). Changing patterns of exhumation and denudation in front of an advancing crustal indenter, Tauern Window (Eastern Alps). *Tectonics*, *36*(6), 1053–1071. https://doi.org/10.1002/2016TC004448

Favaro, S., Schuster, R., Handy, M. R., Scharf, A., & Pestal, G. (2015). Transition from orogen-perpendicular to orogen-parallel exhumation and cooling during crustal indentation—Key constraints from 147 Sm/144 Nd and 87 Rb/87 Sr geochronology (Tauern Window, Alps). *Tectonophysics*, *665*, 1–16. https://doi.org/10.1016/j.tecto.2015.08.037

Fossen, H., & Rykkelid, E. (1990). Shear zone structures in the Øygarden area, West Norway. *Tectonophysics*, *174*(3–4), 385–397. https://doi.org/10.1016/0040-1951(90)90333-4

Frank, W., Höck, V., & Miller, C. (1987). Metamorphic and tectonic history of the central Tauern Window. *Geodynamics of the Eastern Alps*, 34–54.

Frasl, G., & Frank, W. (1964). Exkursion I/2: Mittlere Hohe Tauern. *Mitteilungen Der Geologischen Gesellschaft in Wien*, *57*(1), 17–31.

Frey, M., Desmons, J., & Neubauer, F. (1999). The new metamorphic maps of the Alps: Introduction. *Schweizerische Mineralogische Und Petrographische Mitteilungen*, *79*, 1–4.

Froitzheim, N., Schmid, S. M., & Conti, P. (1994). Repeated change from crustal shortening to orogen-parallel extension in the Austroalpine units of Graubünden. *Eclogae Geologicae Helvetiae*, *87*(2), 559–612.

Girault, J. B., Bellahsen, N., Boutoux, A., Rosenberg, C. L., Nanni, U., Verlaguet, A., & Beyssac, O. (2020). The 3-D thermal structure of the Helvetic Nappes of the European Alps: Implications for collisional processes. *Tectonics*, *39*(3), 183. https://doi.org/10.1029/2018TC005334

Goffé, B., Bousquet, R., Henry, P., & Le Pichon, X. (2003). Effect of the chemical composition of the crust on the metamorphic evolution of orogenic wedges. *Journal of Metamorphic Geology*, *21*(2), 123–141. https://doi.org/10.1046/j.1525-1314.2003.00422.x

Goscombe, B. (1991). Intense non-coaxial shear and the development of mega-scale sheath folds in the Arunta Block, Central Australia. *Journal of Structural Geology*, *13*(3), 299–318. https://doi.org/10.1016/0191-8141(91)90130-B

Groß, P., Handy, M. R., John, T., Pestal, G., & Pleuger, J. (2020). Crustal-scale sheath folding at HP conditions in an exhumed Alpine subduction zone (Tauern Window, Eastern Alps). *Tectonics*, *39*(2). https://doi.org/10.1029/2019TC005942

Groß, P., Pleuger, J., Handy, M., Germer, M., & John, T. (2020). Raman spectroscopy of carbonaceous matter on metasediments from the central Tauern Window (Eastern Alps). GFZ Data Services.

Handy, M. R., Schmid, S. M., Bousquet, R., Kissling, E., & Bernoulli, D. (2010). Reconciling plate-tectonic reconstructions of Alpine Tethys with the geological-geophysical record of spreading and subduction in the Alps. *Earth-Science Reviews*, *102*(3), 121–158. https://doi.org/10.1016/j.earscirev.2010.06.002

Handy, M. R., Ustaszewski, K., & Kissling, E. (2015). Reconstructing the Alps-Carpathians-Dinarides as a key to understanding switches in subduction polarity, slab gaps and surface motion. *International Journal of Earth Sciences*, *104*(1), 1–26. https://doi.org/10.1007/s00531-014-1060-3

Henderson, J. R. (1981). Structural analysis of sheath folds with horizontal X-axes, northeast Canada. *Journal of Structural Geology*, *3*(3), 203–210. https://doi.org/10.1016/0191-8141(81)90016-X

Höck, V. (1980). Distribution maps of minerals of the Alpine metamorphism in the penninic Tauern window, Austria. *Mitteilungen Der Österreichischen Geologischen Gesellschaft*, *71*(72), 119–127.

Höck, V., Ślączka, A., & Uchman, A. (2006). New biostratigraphic and palaeoenvironmental data on metamorphosed limestones from the northern margin of the Tauern Window (Eastern Alps, Austria). *Austrian Journal of Earth Sciences*, *99*, 42–56.

Hoernes, S., & Friedrichsen, H. (1974). Oxygen isotope studies on metamorphic rocks of the Western Hohe Tauern Area (Austria). *Schweizerische Mineralogische Und Petrographische Mitteilungen*, *54*, 769–788.

Hoinkes, G., Koller, F., Rantitsch, G., Dachs, E., Höck, V., Neubauer, F., & Schuster, R. (1999). Alpine metamorphism of the Eastern Alps. *Schweizerische Mineralogische Und Petrographische Mitteilungen*, *79*(1), 155–181.

Hoschek, G. (2001). Thermobarometry of metasediments and metabasites from the Eclogite zone of the Hohe Tauern, Eastern Alps, Austria. *Lithos*, *59*(3), 127–150. https://doi.org/10.1016/S0024-4937(01)00063-9

Inger, S., & Cliff, R. A. (1994). Timing of metamorphism in the Tauern Window, Eastern Alps: Rb-Sr ages and fabric formation. *Journal of Metamorphic Geology*, *12*(5), 695–707. https://doi.org/10.1111/j.1525-1314.1994.tb00052.x

Kirilova, M., Toy, V., Rooney, J. S., Giorgetti, C., Gordon, K. C., Collettini, C., & Takeshita, T. (2018). Structural disorder of graphite and implications for graphite thermometry. *Solid Earth*, *9*(1), 223. https://doi.org/10.5194/se-9-223-2018

Koller, F., & Pestal, G. (2003). Die ligurischen Ophiolite der Tarntaler Berge und der Matreier Schuppenzone. Geologische Bundesanstalt – Arbeitstagung 2003: Blatt 148 Brenner, 65–76.

Kossak-Glowczewski, J., Froitzheim, N., Nagel, T. J., Pleuger, J., Keppler, R., Leiss, B., & Régent, V. (2017). Along-strike shear-sense reversal in the Vals-Scaradra Shear Zone at the front of the Adula Nappe (Central Alps, Switzerland). *Swiss Journal of Geosciences*, *110*(2), 677–697. https://doi.org/10.1007/s00015-017-0270-7

Kouketsu, Y., Mizukami, T., Mori, H., Endo, S., Aoya, M., Hara, H., Nakamura, D., & Wallis, S. (2014). A new approach to develop the Raman carbonaceous material geothermometer for low-grade metamorphism using peak width. *Island Arc*, *23*(1), 33–50. https://doi.org/10.1111/iar.12057

Kurz, W., Handler, R., & Bertoldi, C. (2008). Tracing the exhumation of the Eclogite Zone (Tauern Window, Eastern Alps) by 40Ar/39Ar dating of white mica in eclogites. *Swiss Journal of Geosciences*, *101*(1), 191–206. https://doi.org/10.1007/s00015-008-1281-1

Kurz, W., Neubauer, F., & Genser, J. (1996). Kinematics of Penninic nappes (Glockner Nappe and basement-cover nappes) in the Tauern Window (Eastern Alps, Austria) during subduction and Penninic-Austroalpine collision. *Eclogae Geologicae Helvetiae*, *89*(1), 573–605.

Kurz, W., Neubauer, F., Genser, J., & Dachs, E. (1998). Alpine geodynamic evolution of passive and active continental margin sequences in the Tauern Window (eastern Alps, Austria, Italy): A review. *Geologische Rundschau*, *87*(2), 225–242. https://doi.org/10.1007/s005310050204

Lacassin, R., & Mattauer, M. (1985). Kilometre-scale sheath fold at Mattmark and implications for transport direction in the Alps. *Nature*, *315*(6022), 739–742.

Lahfid, A., Beyssac, O., Deville, E., Negro, F., Chopin, C., & Goffé, B. (2010). Evolution of the Raman spectrum of carbonaceous material in low-grade metasediments of the Glarus Alps (Switzerland). *Terra Nova*, *22*(5), 354–360. https://doi.org/10.1111/j.1365-3121.2010.00956.x

Lambert, R. S. J. (1970). A potassium-argon study of the margin of the Tauernfenster at Döllach, Austria. *Eclogae Geologicae Helvetiae*, *63*, 197–205.

Lemoine, M. (2003). Schistes lustrés from Corsica to Hungary: Back to the original sediments and tentative dating of partly azoic metasediments. *Bulletin De La Société Géologique De France*, *174*(3), 197–209.

Lünsdorf, N. K., Dunkl, I., Schmidt, B. C., Rantitsch, G., & von Eynatten, H. (2017). Towards a higher comparability of geothermometric data obtained by Raman spectroscopy of carbonaceous material. Part 2: A revised geothermometer. *Geostandards and Geoanalytical Research*, *41*(4), 593–612.

Luth, S. W., & Willingshofer, E. (2008). Mapping of the post-collisional cooling history of the Eastern Alps. *Swiss Journal of Geosciences*, *101*(1), 207–223. https://doi.org/10.1007/s00015-008-1294-9

Marques, F. O., & Cobbold, P. R. (1995). Development of highly non-cylindrical folds around rigid ellipsoidal inclusions in bulk simple shear regimes: Natural examples and experimental modelling. *Journal of Structural Geology*, *17*(4), 589–602. https://doi.org/10.1016/0191-8141(94)00081-A

Marques, F. O., Guerreiro, S. M., & Fernandes, A. R. (2008). Sheath fold development with viscosity contrast: Analogue experiments in bulk simple shear. *Journal of Structural Geology*, *30*(11), 1348–1353. https://doi.org/10.1016/j.jsg.2008.07.001

Maxelon, M., & Mancktelow, N. S. (2005). Three-dimensional geometry and tectonostratigraphy of the Pennine zone, Central Alps, Switzerland and Northern Italy. *Earth-Science Reviews*, *71*(3–4), 171–227. https://doi.org/10.1016/j.earscirev.2005.01.003

Milnes, A. G. (1974). Structure of the Pennine Zone (Central Alps): A new working hypothesis. *Geological Society of America*

Bulletin, *85*(11), 1727–1732. https://doi.org/10.1130/0016-7606(1974)85<1727:SOTPZC>2.0.CO;2

Molnar, P., & England, P. C. (1990). Temperatures, heat flux, and frictional stress near major thrust faults. *Journal of Geophysical Research: Solid Earth*, *95*(B4), 4833–4856. https://doi.org/10.1029/JB095iB04p04833

Mori, H., Mori, N., Wallis, S., Westaway, R., & Annen, C. (2017). The importance of heating duration for Raman CM thermometry: Evidence from contact metamorphism around the Great Whin Sill intrusion, UK. *Journal of Metamorphic Geology*, *35*(2), 165–180. https://doi.org/10.1111/jmg.12225

Mori, N., Wallis, S., & Mori, H. (2015). Graphitization of carbonaceous material in sedimentary rocks on short geologic time-scales: An example from the Kinsho-Zan area, central Japan. *Island Arc*, *24*(2), 119–130. https://doi.org/10.1111/iar.12093

Nagel, T. J., Herwartz, D., Rexroth, S., Münker, C., Froitzheim, N., & Kurz, W. (2013). Lu-Hf dating, petrography, and tectonic implications of the youngest Alpine eclogites (Tauern Window, Austria). *Lithos*, *170*, 179–190. https://doi.org/10.1016/j.lithos.2013.02.008

Oberhänsli, R., Bousquet, R., Engi, M., Goffé, B., Gosso, G., Handy, M. R. et al. (2004). Metamorphic structure of the Alps. CCGM (Commission of the Geological Maps of the World). Paris.

Oxburgh, E. R., Lambert, R. S. J., Baadsgaard, H., & Simons, J. G. (1966). Potassium argon age studies across the south-east margin of the Tauern Window, the Eastern Alps. *Verhandlungen Der Geologischen Bundesanstalt*, *1966*, 17–33.

Peacock, S. M. (1996). Thermal and petrologic structure of subduction zones. *Subduction: Top to Bottom*, *96*, 119–133.

Pestal, G., & Hellerschmidt-Alber, J. (2011). über geologische Aufnahmen auf Blatt 154 Rauris. *Jahrbuch Der Geologischen Bundesanstalt*, *151*(1+2), 142–147. Bericht 2009 und 2010.

Ratschbacher, L., Dingeldey, C., Miller, C., Hacker, B. R., & McWilliams, M. O. (2004). Formation, subduction, and exhumation of Penninic oceanic crust in the Eastern Alps: Time constraints from 40 Ar/39 Ar geochronology. *Tectonophysics*, *394*(3), 155–170. https://doi.org/10.1016/j.tecto.2004.08.003

Ratschbacher, L., Frisch, W., Linzer, H.-G., & Merle, O. (1991). Lateral extrusion in the Eastern Alps, part 2: Structural analysis. *Tectonics*, *10*(2), 257–271. https://doi.org/10.1029/90TC02623

Reber, J. E., Dabrowski, M., & Schmid, D. W. (2012). Sheath fold formation around slip surfaces. *Terra Nova*, *24*(5), 417–421. https://doi.org/10.1111/j.1365-3121.2012.01081.x

Reddy, S. M., Cliff, R. A., & East, R. (1993). Thermal history of the Sonnblick Dome, south-east Tauern Window, Austria: Implications for heterogeneous uplift within the Pennine basement. *Geologische Rundschau*, *82*(4), 667–675. https://doi.org/10.1007/BF00191494

Reich, S., & Thomsen, C. (2004). Raman spectroscopy of graphite. *Philosophical Transactions of the Royal Society of London. Series A: Mathematical, Physical and Engineering Sciences*, *362*(1824), 2271–2288. https://doi.org/10.1098/rsta.2004.1454

Reitz, E., Höll, R., Hupak, W., & Mehltretter, C. (1990). Palynologischer Nachweis von Unterkreide in der Jüngeren (Oberen) Schieferhülle des Tauernfensters (Ostalpen). *Jahrbuch Der Geologischen Bundesanstalt*, *133*(4), 611–618.

Rosenberg, C. L., Brun, J.-P., Cagnard, F., & Gapais, D. (2007). Oblique indentation in the Eastern Alps: Insights from laboratory experiments. *Tectonics*, *26*(2). https://doi.org/10.1029/2006TC001960

Rosenberg, C. L., Schneider, S., Scharf, A., Bertrand, A., Hammerschmidt, K., Rabaute, A., & Brun, J.-P. (2018). Relating collisional kinematics to exhumation processes in the Eastern Alps.

Earth-Science Reviews, *176*, 311–344. https://doi.org/10.1016/j.earscirev.2017.10.013

Sander, B. (1911). Geologische Studien am Westende der Hohen Tauern. Denkschriften Der Kaiserlichen Akademie Der Wissenschaften, 82.

Scharf, A., Handy, M. R., Favaro, S., Schmid, S. M., & Bertrand, A. (2013). Modes of orogen-parallel stretching and extensional exhumation in response to microplate indentation and roll-back subduction (Tauern Window, Eastern Alps). *International Journal of Earth Sciences*, *102*(6), 1627–1654. https://doi.org/10.1007/s00531-013-0894-4

Scharf, A., Handy, M. R., Schmid, S. M., Favaro, S., Sudo, M., Schuster, R., & Hammerschmidt, K. (2016). Grain-size effects on the closure temperature of white mica in a crustal-scale extensional shear zone—Implications of in-situ 40Ar/39Ar laser-ablation of white mica for dating shearing and cooling (Tauern Window, Eastern Alps). *Tectonophysics*, *674*, 210–226. https://doi.org/10.1016/j.tecto.2016.02.014

Scharf, A., Handy, M. R., Ziemann, M. A., & Schmid, S. M. (2013). Peak-temperature patterns of polyphase metamorphism resulting from accretion, subduction and collision (eastern Tauern Window, European Alps)–A study with Raman microspectroscopy on carbonaceous material (RSCM). *Journal of Metamorphic Geology*, *31*(8), 863–880. https://doi.org/10.1111/jmg.12048

Schmid, S. M., Fügenschuh, B., Kissling, E., & Schuster, R. (2004). Tectonic map and overall architecture of the Alpine orogen. *Eclogae Geologicae Helvetiae*, *97*(1), 93–117. https://doi.org/10.1007/s00015-004-1113-x

Schmid, S. M., Scharf, A., Handy, M. R., & Rosenberg, C. L. (2013). The Tauern Window (Eastern Alps, Austria): A new tectonic map, with cross-sections and a tectonometamorphic synthesis. *Swiss Journal of Geosciences*, *106*(1), 1–32. https://doi.org/10.1007/s00015-013-0123-y

Schmidt, K. (2015). Microstructural and thermobarometric investigations of high-pressure mineral assemblages in metapelites of the Modereck Nappe Complex (Tauern Window, Austria). Freie Universität Berlin.

Searle, M. P., & Alsop, G. I. (2007). Eye-to-eye with a mega-sheath fold: A case study from Wadi Mayh, northern Oman Mountains. *Geology*, *35*(11), 1043–1046. https://doi.org/10.1130/G23884A.1

Selverstone, J. (1993). Micro-to macroscale interactions between deformational and metamorphic processes, Tauern Window, Eastern Alps. *Schweizerische Mineralogische Und Petrographische Mitteilungen*, *73*(2), 229–239.

Selverstone, J., Spear, F. S., Franz, G., & Morteani, G. (1984). High-pressure metamorphism in the SW Tauern Window, Austria: PT paths from hornblende-kyanite-staurolite schists. *Journal of Petrology*, *25*(2), 501–531. https://doi.org/10.1093/petrology/25.2.501

Smye, A. J., Bickle, M. J., Holland, T. J. B., Parrish, R. R., & Condon, D. J. (2011). Rapid formation and exhumation of the youngest Alpine eclogites: A thermal conundrum to Barrovian metamorphism. *Earth and Planetary Science Letters*, *306*(3–4), 193–204. https://doi.org/10.1016/j.epsl.2011.03.037

Stampfli, G. M., & Borel, G. D. (2004). The TRANSMED Transects in Space and Time: Constraints on the Paleotectonic Evolution of the Mediterranean Domain. In W. Cavazza, F. M. Roure, W. Spakman, G. M. Stampfli, & P. A. Ziegler (Eds.), *The TRANSMED Atlas. The Mediterranean Region from Crust to Mantle* (pp. 53–80). Springer.

Steck, A., Epard, J.-L., & Masson, H. (2019). The Maggia nappe: An extruding sheath fold basement nappe in the Lepontine gneiss dome

of the Central Alps. *International Journal of Earth Sciences*, 1–14. https://doi.org/10.1007/s00531-019-01771-1

Steck, A., & Hunziker, J. (1994). The Tertiary structural and thermal evolution of the Central Alps—Compressional and extensional structures in an orogenic belt. *Tectonophysics*, *238*(1–4), 229–254. https://doi.org/10.1016/0040-1951(94)90058-2

Stöckhert, B., Massonne, H.-J., & Nowlan, E. U. (1997). Low differential stress during high-pressure metamorphism: The microstructural record of a metapelite from the Eclogite Zone, Tauern Window, Eastern Alps. *Lithos*, *41*(1–3), 103–118. https://doi.org/10.1016/S0024-4937(97)82007-5

Vollmer, F. W. (1988). A computer model of sheath-nappes formed during crustal shear in the Western Gneiss Region, central Norwegian Caledonides. *Journal of Structural Geology*, *10*(7), 735–743. https://doi.org/10.1016/0191-8141(88)90080-6

Wheeler, J., Reddy, S. M., & Cliff, R. A. (2001). Kinematic linkage between internal zone extension and shortening in more external units in the NW Alps. *Journal of the Geological Society*, *158*(3), 439–443. https://doi.org/10.1144/jgs.158.3.439

Wiederkehr, M., Bousquet, R., Ziemann, M. A., Berger, A., & Schmid, S. M. (2011). 3-D assessment of peak-metamorphic conditions by Raman spectroscopy of carbonaceous material: An example from the margin of the Lepontine dome (Swiss Central Alps). *International Journal of Earth Sciences*, *100*(5), 1029–1063. https://doi.org/10.1007/s00531-010-0622-2

Xypolias, P., & Alsop, G. I. (2014). Regional flow perturbation folding within an exhumation channel: A case study from the Cycladic Blueschists. *Journal of Structural Geology*, *62*, 141–155. https://doi.org/10.1016/j.jsg.2014.02.001

Zimmermann, R., Hammerschmidt, K., & Franz, G. (1994). Eocene high pressure metamorphism in the Penninic units of the Tauern Window (Eastern Alps): Evidence from 40Ar-39Ar dating and petrological investigations. *Contributions to Mineralogy and Petrology*, *117*(2), 175–186. https://doi.org/10.1007/BF00286841

SUPPORTING INFORMATION

Additional supporting information may be found online in the Supporting Information section.

Figure S1. Examples of semi-quantitative projection of RSCM data into cross-sections.

Figure S2. Map of the central Tauern Window with sample locations for RSCM analysis.

Figure S3. Enlarged, high-resolution version of RSCM peak-temperature map of the central Tauern Window.

Figure S4. Profiles of the central Tauern Window with sample locations for RSCM analysis.

Figure S5. Enlarged, high-resolution version of profiles with RSCM temperatures of the central Tauern Window.

Appendix S1. Compilation of Barrovian peak-temperature contours.

Appendix S2. Cross-section construction, data projection and contour interpolation.

How to cite this article: Groß P, Pleuger J, Handy MR, Germer M, John T. Evolving temperature field in a fossil subduction channel during the transition from subduction to collision (Tauern Window, Eastern Alps). *J Metamorph Geol* 2020;00:1–23. https://doi.org/10.1111/jmg.12572